SCATTERING FROM MULTIPLE DISCONTINUITIES IN WAVEGUIDES

BY

GLENN A. GESELL

A Thesis

Submitted to the Faculty of Graduate Studies

in Partial Fulfillment of the Requirements

for the Degree of

MASTER OF SCIENCE

Department of Electrical and Computer Engineering

University of Manitoba

Winnipeg, Manitoba

ISBN 0-315-77961-6

Canada

SCATTERING FROM MULTIPLE DISCONTINUITIES IN WAVEGUIDES

BY

GLENN A. GESELL

A Thesis submitted to the Faculty of Graduate Studies of the University of Manitoba in partial fulfillment of the requirements for the degree of

MASTER OF SCIENCE

ABSTRACT

A general formulation for the scattering from multiple discontinuities in waveguides is presented in this thesis. The global scattering matrices are derived from the coupled sets of truncated linear equations obtained by expanding the corresponding fields in terms of vector eigenfunctions and imposing the boundary conditions at each junction. The analysis takes into account the near field coupling and higher order mode interaction between the discontinuities. A recurrence procedure used in derivation of the scattering matrices gives the proposed formulation a significant computational advantage over the commonly used cascading techniques. The conditions for a good overall convergence are illustrated for step-discontinuities in circular waveguides. Numerical results are presented for a thick iris in a circular waveguide and for multiple-step transformers in circular waveguides. Improved designs for iris matched dielectric windows are also calculated and presented.

ACKNOWLEDGEMENTS

The author wishes to express his sincere appreciation to Dr. I. R. Ciric for his advice and encouragement throughout the course of this research.

Thanks are also due to my family and friends for all their support and encouragement.

LIST OF FIGURES

Page

Fig. 2.1. Section with multiple waveguide discontinuities. 5

Fig. 3.1. Geometry of a thick iris. 18

Fig. 3.2. Magnitude of the reflection coefficient as a function of P with $M = N(a/b) = 20$, for a thick iris with $a = 2b$ and $ka = 3.2$. 19

Fig. 3.3. Magnitude of the reflection coefficient as a function of M $(P = M)$ for a thick iris with $a = 2b$, $L/a = 0.01$, and $ka = 3.2$. 20

Fig. 3.4. Convergence of the magnitude of the reflection coefficient as a function of M for a thick iris with $a = 2b$, $L/a = 0.01$, and $ka = 2.4$. 21

Fig. 3.5. Convergence of the magnitude of the reflection coefficient as a function of M for a thick iris with $a = 2b$, $L/a = 0.1$, and $ka = 2.4$. 22

Fig. 3.6. Convergence of the magnitude of the reflection coefficient as a function of M for a thick iris with $a = 2b$, $L/a = 0.01$, and $ka = 3.2$. 23

Fig. 3.7. Geometry of an iris matched dielectric window. 31

Fig. 3.8. Optimum iris radius as a function of the normalized frequency for an iris matched dielectric window with $\varepsilon_r = 2.8$ and $L_i = L$. 32

Fig. 3.9. Return loss as a function of the normalized frequency for an iris matched dielectric window optimized for $f_o / f_c = 1.1$, 1.3, and 1.5 with $\varepsilon_r = 2.8$, $L/a = 0.01$, and $L_i = L$. 33

Page

Fig. 3.10. Return loss as a function of the normalized frequency for an iris matched dielectric window optimized for f_o / f_c = 1.1, 1.3, and 1.5 with $\varepsilon_r = 2.8$, $L/a = 0.02$, and $L_i = L$. 34

Fig. 3.11. Return loss as a function of the normalized frequency for an iris matched dielectric window optimized for f_o / f_c = 1.1, 1.3, and 1.5 with $\varepsilon_r = 2.8$, $L/a = 0.03$, and $L_i = L$. 35

Fig. 3.12. Return loss as a function of the normalized frequency for an iris matched dielectric window optimized for f_o / f_c = 1.1, 1.3, and 1.5 with $\varepsilon_r = 2.8$, $L/a = 0.04$, and $L_i = L$. 36

Fig. 3.13. Optimum iris radius as a function of the normalized frequency for an iris matched dielectric window with $\varepsilon_r = 2.8$ and $L_i = 5L$. 37

Fig. 3.14. Return loss as a function of the normalized frequency for an iris matched dielectric window optimized for f_o / f_c = 1.1, 1.3, and 1.5 with $\varepsilon_r = 2.8$, $L/a = 0.01$, and $L_i = 5L$. 38

Fig. 3.15. Return loss as a function of the normalized frequency for an iris matched dielectric window optimized for f_o / f_c = 1.1, 1.3, and 1.5 with $\varepsilon_r = 2.8$, $L/a = 0.02$, and $L_i = 5L$. 39

Fig. 3.16. Return loss as a function of the normalized frequency for an iris matched dielectric window optimized for f_o / f_c = 1.1, 1.3, and 1.5 with $\varepsilon_r = 2.8$, $L/a = 0.03$, and $L_i = 5L$. 40

Fig. 3.17. Return loss as a function of the normalized frequency for an iris matched dielectric window optimized for f_o / f_c = 1.1, 1.3, and 1.5 with $\varepsilon_r = 2.8$, $L/a = 0.04$, and $L_i = 5L$. 41

Page

Fig. 4.1. Magnitude of the reflection coefficient as a function of P for a thick iris with $a = 1.338b$ and $ka = 2.4$. 57

Fig. 4.2. Magnitude of the reflection coefficient as a function of P for a thick iris with $a = 1.338b$ and $ka = 3.2$. 58

Fig. 4.3 Geometry of a circular waveguide step transformer.
a) two-section transformer
b) four-section transformer 64

Fig. 4.4 VSWR of a two-section transformer with dimensions as in Table 4.9. 66

Fig. 4.4 VSWR of a four-section transformer with dimensions as in Table 4.9. 67

LIST OF TABLES

Page

Table 3.1. Reflection coefficient as a function of L/a for a thick iris with $a = 2b$ and $ka = 3.2$. 24

Table 3.2. Transmission coefficient as a function of L/a for a thick iris with $a = 2b$ and $ka = 3.2$. 24

Table 3.3. Comparison of the reflection coefficient as a function of L for a thick iris with $a = 0.50175$ in, $b = 0.25$ in, and $f = 9$ GHz. 26

Table 3.4. Comparison of the transmission coefficient as a function of L for a thick iris with $a = 0.50175$ in, $b = 0.25$ in, and $f = 9$ GHz. 26

Table 3.5. Comparison of the reflection coefficient as a function of L for a thick iris with $a = 0.50175$ in, $b = 0.25$ in, and $f = 12$ GHz. 27

Table 3.6. Comparison of the transmission coefficient as a function of L for a thick iris with $a = 0.50175$ in, $b = 0.25$ in, and $f = 12$ GHz. 27

Table 3.7. Comparison of the reflection coefficient as a function of L for a thick iris with $a = 0.50175$ in, $b = 0.375$ in, and $f = 9$ GHz. 28

Table 3.8. Comparison of the transmission coefficient as a function of L for a thick iris with $a = 0.50175$ in, $b = 0.375$ in, and $f = 9$ GHz. 28

Table 3.9. Comparison of the reflection coefficient as a function of L for a thick iris with $a = 0.50175$ in, $b = 0.375$ in, and $f = 12$ GHz. 29

Table 3.10. Comparison of the transmission coefficient as a function of L for a thick iris with $a = 0.50175$ in, $b = 0.375$ in, and $f = 12$ GHz. 29

Page

Table 3.11. Comparison of the number and size of full matrix inversions needed for matched dielectric window analysis. 43

Table 3.12. Comparison of the minimum number of full matrix multiplications and inversions needed to calculate $\underline{\underline{S}}_{11}$ and $\underline{\underline{S}}_{21}$ for N discontinuities. 43

Table 4.1. Comparison of the reflection coefficient as a function of L for a thick iris with $a = 0.50175$ in, $b = 0.25$ in, and $f = 9$ GHz. 59

Table 4.2. Comparison of the transmission coefficient as a function of L for a thick iris with $a = 0.50175$ in, $b = 0.25$ in, and $f = 9$ GHz. 59

Table 4.3. Comparison of the reflection coefficient as a function of L for a thick iris with $a = 0.50175$ in, $b = 0.25$ in, and $f = 12$ GHz. 60

Table 4.4. Comparison of the transmission coefficient as a function of L for a thick iris with $a = 0.50175$ in, $b = 0.25$ in, and $f = 12$ GHz. 60

Table 4.5. Comparison of the reflection coefficient as a function of L for a thick iris with $a = 0.50175$ in, $b = 0.375$ in, and $f = 9$ GHz. 61

Table 4.6. Comparison of the transmission coefficient as a function of L for a thick iris with $a = 0.50175$ in, $b = 0.375$ in, and $f = 9$ GHz. 61

Table 4.7. Comparison of the reflection coefficient as a function of L for a thick iris with $a = 0.50175$ in, $b = 0.375$ in, and $f = 12$ GHz. 62

Table 4.8. Comparison of the transmission coefficient as a function of L for a thick iris with $a = 0.50175$ in, $b = 0.375$ in, and $f = 12$ GHz. 62

Table 4.9. Dimensions for step transformer designs. 65

LIST OF PRINCIPAL SYMBOLS

E	electric field
H	magnetic field
t	refers to transverse components of the electric and magnetic field
A	forward modal coefficients
B	backward modal coefficients
e	modal electric field functions
$\boldsymbol{h}$	modal magnetic field functions
γ	propagation constant
S	waveguide cross section
δ_{mn}	Kronecker delta (= 0 if $m \neq n$; = 1 if $m = n$)
L	length of waveguide section
$\underline{\underline{G}}, \underline{\underline{H}}, \underline{\underline{P}}, \underline{\underline{K}}$	modal coupling matrices
$\underline{\underline{S}}_{11}$	reflection matrix
$\underline{\underline{S}}_{21}$	transmission matrix
$\underline{\underline{I}}$	unit matrix
r, ϕ, z	circular cylindrical coordinates
j	$\sqrt{-1}$
ω	angular frequency
ε	permittivity
μ	permeability
k	wave number
f	frequency
f_c	cutoff frequency

TABLE OF CONTENTS

	Page
ABSTRACT	i
ACKNOWLEDGEMENTS	ii
LIST OF FIGURES	iii
LIST OF TABLES	vi
LIST OF PRINCIPAL SYMBOLS	viii
CHAPTER 1 INTRODUCTION	1
CHAPTER 2 ANALYSIS OF MULTIPLE DISCONTINUITIES IN WAVEGUIDES	4
2.1 MODAL EXPANSIONS OF THE FIELDS	4
2.2 BOUNDARY CONDITIONS AT THE DISCONTINUITY PLANES	6
2.3 MATRIX EQUATIONS FOR THE DISCONTINUITIES	7
2.3.1 Boundary Enlargement Discontinuities	7
2.3.2 Boundary Reduction Discontinuities	9
2.4 SCATTERING MATRIX FORMULATION	11
2.5 SYMMETRIC DISCONTINUITIES	13
CHAPTER 3 APPLICATION TO CIRCULAR WAVEGUIDES	15
3.1 MODAL FUNCTION EXPRESSIONS	15
3.2 MODAL COUPLING INTEGRALS	15
3.3 NUMERICAL RESULTS	17
3.3.1 Convergence and Accuracy	17
3.3.2 Application to Iris Matched Dielectric Windows	30

Page

CHAPTER 4 IMPROVED MODELLING WITH RESTRICTED HIGHER ORDER MODE INTERACTION 44

4.1 MODAL EXPANSIONS OF THE FIELDS 45

4.2 BOUNDARY CONDITIONS AT THE DISCONTINUITY PLANES 46

4.3 MATRIX EQUATIONS FOR THE DISCONTINUITIES 47

4.3.1 Boundary Enlargement Discontinuities 47

4.3.2 Boundary Reduction Discontinuities 50

4.4 SCATTERING MATRIX FORMULATION 53

4.5 NUMERICAL RESULTS FOR CIRCULAR WAVEGUIDES 56

4.5.1 Convergence and Accuracy 56

4.5.2 Application to Step Transformers 63

CHAPTER 5 CONCLUSIONS AND RECOMMENDATIONS 68

APPENDIX IDENTITIES FOR COUPLING MATRICES 70

REFERENCES 71

CHAPTER 1

INTRODUCTION

The analysis of waveguide discontinuities is a classic electromagnetic theory and microwave engineering problem with application to the design of microwave components and antennas. Multiple-step discontinuities in waveguides are encountered in filters, transformers, irises, directional couplers [1], mode converters [2], and the modelling of horn antennas [3].

Structures with multiple waveguide discontinuities are typically analyzed by cascading individual discontinuities. Methods for cascading generalized scattering matrices are described by James [2], and Chu and Itoh [4]. Cascading can also be performed using the transmission matrix representation, but this method has some disadvantages not encountered with the generalized scattering matrix approach. The method can be numerically unstable when too many higher order modes are included in the waveguide sections between the discontinuities or the overall length of the waveguide sections is too large [5]. Also, the transmission matrix method requires the field expansions in each waveguide to have the same number of modes which may violate the criterion to avoid the relative convergence phenomenon [6], [7]. This restriction has been overcome using an improved transmission matrix formulation proposed by Mansour and MacPhie [8]. Cascading with an admittance matrix formulation has also been proposed [9].

Problems relative to multiple discontinuities in waveguides have been solved by numerous techniques. Rozzi and Mecklenbräuker [10] extended the variational method to study interacting irises and steps in waveguides. De Smedt and Denturk [11] determined the scattering from symmetric double discontinuities using the moment method with point matching. Double discontinuities have been treated using the moment method with the Galerkin technique by Hamid *et. al.* [12], Datta *et. al.* [13], and Scharstein and Adams [14]. An earlier mode matching technique was applied to double discontinuities by

Clarricoats and Slinn [15]; however, the solution required large matrix operations which Huckle and Masterman [16] avoided by reducing the sets of equations and using back substitution. An admittance matrix formulation based on modal analysis has been used by Alessandri *et. al.* [9] to solve for a special class of double discontinuities. All the mode matching based techniques may suffer from the relative convergence phenomenon which is eliminated by using an appropriate ratio of modal terms in the waveguide field expansions [6], [7].

The purpose of this thesis is to present a solution for multiple-step waveguide discontinuities where the scattering parameters are directly calculated by simultaneously solving the multiple discontinuities rather than by cascading discontinuities.

In Chapter 2, a general formulation for the scattering from multiple waveguide discontinuities is presented. The formulation is based on the modal analysis technique [17] where the electric and magnetic fields in each waveguide section are expressed as an exact expansion of orthonormal modes and the boundary conditions on the tangential field components are enforced over each discontinuity plane. Analytic expressions for the scattering matrices are derived from the truncated linear equations formed by applying the mode orthogonality.

In Chapter 3, multiple-step discontinuities in circular waveguides will be considered for quantitative illustrations. A thick iris in a circular waveguide is analyzed in detail to verify the convergence and accuracy of the formulation. Numerical results are compared with data available in the literature. Also, application is made to improve designs for iris matched dielectric windows.

In Chapter 4, a modified formulation for the scattering from multiple waveguide discontinuities is presented. The higher order modes that are excited at the discontinuities but do not effectively interact with the adjacent discontinuities are matched terminated in the analysis. A thick iris in a circular waveguide is studied quantitatively to determine a criterion for choosing the number of interacting modes between circular waveguide

discontinuities. The accuracy of the formulation is verified for a thick iris in a circular waveguide and for circular waveguide step transformers by comparing numerical results with data available in the literature.

The conclusions and recommendations are presented in Chapter 5.

CHAPTER 2

ANALYSIS OF MULTIPLE DISCONTINUITIES IN WAVEGUIDES

The problem of multiple discontinuities in waveguides is discussed in this chapter. Consider the multiple-step discontinuities shown in Fig. 2.1. There are N transverse discontinuities with N+1 waveguide regions. An arbitrary multi-mode incident field is assumed from waveguide 1.

Determining the electromagnetic scattering for the multiple discontinuities begins with expressing the electric and magnetic fields in each waveguide section as an exact expansion of orthonormal modes and enforcing the boundary conditions on the tangential fields over each discontinuity plane. The scattering matrices are derived from the truncated linear equations formed by applying the mode orthogonality.

2.1 Modal Expansions of the Fields

The total transverse electric and magnetic fields can be written in modal form as follows:

in the 1st region

$$\boldsymbol{E}_{t1} = \sum_m \left(A_{1m}\, e^{-\gamma_{1m}(z+z_1)} + B_{1m}\, e^{\gamma_{1m}(z+z_1)}\right)\boldsymbol{e}_{1m}$$

$$\boldsymbol{H}_{t1} = \sum_m \left(A_{1m}\, e^{-\gamma_{1m}(z+z_1)} - B_{1m}\, e^{\gamma_{1m}(z+z_1)}\right)\boldsymbol{h}_{1m}, \tag{2.1}$$

in the jth region ($j = 2, \ldots, N$)

$$\boldsymbol{E}_{tj} = \sum_m \left(A_{jm}\, e^{-\gamma_{jm}(z+z_{j-1})} + B_{jm}\, e^{\gamma_{jm}(z+z_j)}\right)\boldsymbol{e}_{jm}$$

$$\boldsymbol{H}_{tj} = \sum_m \left(A_{jm}\, e^{-\gamma_{jm}(z+z_{j-1})} - B_{jm}\, e^{\gamma_{jm}(z+z_j)}\right)\boldsymbol{h}_{jm}, \tag{2.2}$$

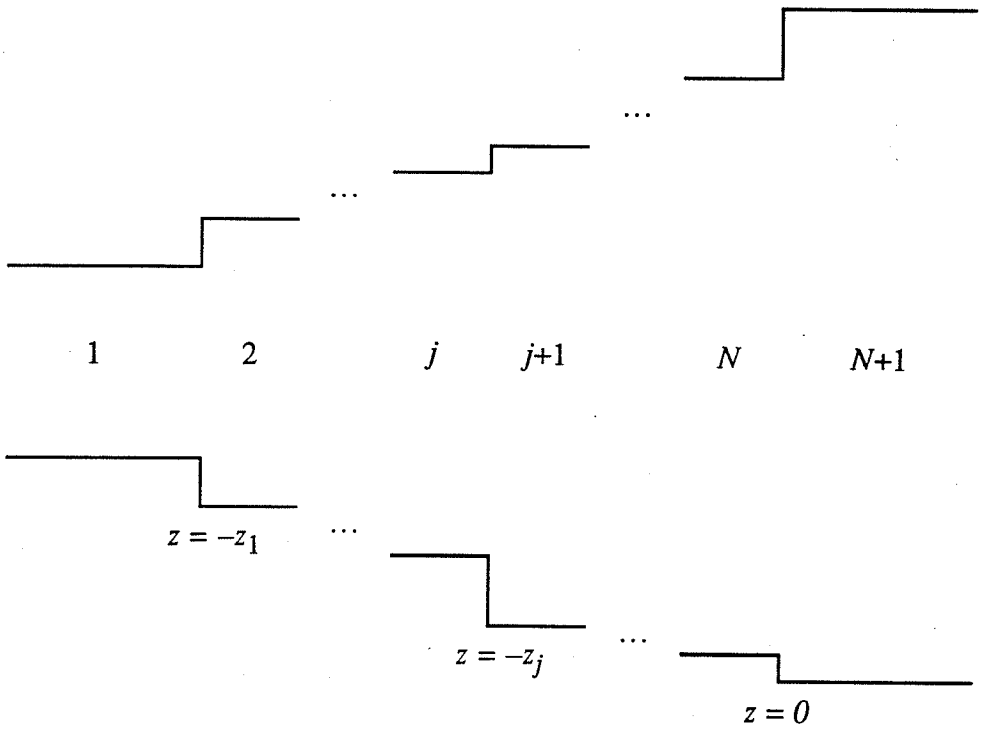

Fig. 2.1. Section with multiple waveguide discontintuities.

and in the N+1th region

$$\boldsymbol{E}_{t,N+1} = \sum_m A_{N+1,m}\, e^{-\gamma_{N+1,m} z}\, \boldsymbol{e}_{N+1,m}$$

$$\boldsymbol{H}_{t,N+1} = \sum_m A_{N+1,m}\, e^{-\gamma_{N+1,m} z}\, \boldsymbol{h}_{N+1,m}. \tag{2.3}$$

A_{im} and B_{im} are the forward and the backward complex coefficients, respectively, of the mth mode in the ith region, γ_{im} is the propagation constant, and $\boldsymbol{e}_{im}$ and $\boldsymbol{h}_{im}$ are the corresponding transverse electric and magnetic field functions of the mth mode. The modal field functions form an orthonormal set, *i.e.*,

$$\langle \boldsymbol{e}_{im}, \boldsymbol{h}_{in} \rangle_{S_i} = \int_{S_i} (\boldsymbol{e}_{im} \times \boldsymbol{h}_{in}) \cdot d\boldsymbol{s} = \delta_{mn} \tag{2.4}$$

where S_i is the ith waveguide cross section, and δ_{mn} is the Kronecker delta.

2.2 Boundary Conditions at the Discontinuity Planes

At each discontinuity plane, the transverse fields must be continuous over each aperture and the tangential electric field must be zero on the walls. The continuity of the transverse electric and magnetic field intensities over each aperture cross section are expressed as follows:

at $z = -z_1$

$$\sum_m (A_{1m} + B_{1m})\boldsymbol{e}_{1m} = \sum_m (A_{2m} + B_{2m}\, e^{-\gamma_{2m} L_2})\boldsymbol{e}_{2m}$$

$$\sum_m (A_{1m} - B_{1m})\boldsymbol{h}_{1m} = \sum_m (A_{2m} - B_{2m}\, e^{-\gamma_{2m} L_2})\boldsymbol{h}_{2m}, \tag{2.5}$$

at $z = -z_j$ $(j = 2, \ldots, N-1)$

$$\sum_m (A_{jm}\, e^{-\gamma_{jm} L_j} + B_{jm})\boldsymbol{e}_{jm} = \sum_m (A_{j+1,m} + B_{j+1,m}\, e^{-\gamma_{j+1,m} L_{j+1}})\boldsymbol{e}_{j+1,m}$$

$$\sum_m (A_{jm}\, e^{-\gamma_{jm} L_j} - B_{jm})\boldsymbol{h}_{jm} = \sum_m (A_{j+1,m} - B_{j+1,m}\, e^{-\gamma_{j+1,m} L_{j+1}})\boldsymbol{h}_{j+1,m}, \tag{2.6}$$

and at $z = 0$

$$\sum_m \left(A_{Nm}\, e^{-\gamma_{Nm} L_N} + B_{Nm}\right) \boldsymbol{e}_{Nm} = \sum_m A_{N+1,m}\, \boldsymbol{e}_{N+1,m}$$

$$\sum_m \left(A_{Nm}\, e^{-\gamma_{Nm} L_N} - B_{Nm}\right) \boldsymbol{h}_{Nm} = \sum_m A_{N+1,m}\, \boldsymbol{h}_{N+1,m} \tag{2.7}$$

where

$$L_i \equiv -z_i + z_{i-1} \quad (i = 2, \ldots, N). \tag{2.8}$$

2.3 Matrix Equations for the Discontinuities

The orthogonality of the modes is applied to the field continuity equations, (2.5)-(2.7), to form linear equations that are truncated and expressed in matrix form. The boundary enlargement and reduction discontinuity cases are handled separately in order to properly include the boundary condition on the transverse walls [17], [18]. For a boundary reduction discontinuity, the cross section of the waveguide section following the discontinuity is encompassed by the cross section of the waveguide section preceding the discontinuity. The boundary enlargement case is illustrated in Fig. 2.1.

As a result of the truncations, the solution to the scattering problem will be an approximate solution where the accuracy is dependent on the number of modes selected in each region. Choosing the ratio of modes approximately equal to the ratio of the waveguide dimensions prevents the relative convergence phenomenon where the solution may converge to an incorrect result or may not converge at all [6], [7].

2.3.1 Boundary Enlargement Discontinuities

For the boundary enlargement case, at each discontinuity we take the vector product of the terms in the electric field continuity equation with a magnetic mode function from the following waveguide section, and the vector product of the terms in the magnetic field continuity equation with an electric mode function from the preceding waveguide section. Applying the orthogonality of the modes, equations (2.5)-(2.7) become:

at $z = -z_1$

$$\sum_m (A_{1m} + B_{1m})\langle \boldsymbol{e}_{1m}, \boldsymbol{h}_{2n}\rangle_{S_1} = F_{2n}\cosh(\gamma_{2n}L_2) + D_{2n}\sinh(\gamma_{2n}L_2) \quad (n=1, 2, 3...)$$

$$A_{1n} - B_{1n} = \sum_m (D_{2m}\cosh(\gamma_{2m}L_2) + F_{2m}\sinh(\gamma_{2m}L_2))\langle \boldsymbol{e}_{1n}, \boldsymbol{h}_{2m}\rangle_{S_1} \quad (n=1, 2, 3...), \quad (2.9)$$

at $z = -z_j$ $(j \neq 1, N)$

$$\sum_m F_{jm}\langle \boldsymbol{e}_{jm}, \boldsymbol{h}_{j+1,n}\rangle_{S_j} = F_{j+1,n}\cosh(\gamma_{j+1,n}L_{j+1}) + D_{j+1,n}\sinh(\gamma_{j+1,n}L_{j+1}) \quad (n=1, 2, 3...)$$

$$D_{jn} = \sum_m (D_{j+1,m}\cosh(\gamma_{j+1,m}L_{j+1}) + F_{j+1,m}\sinh(\gamma_{j+1,m}L_{j+1}))\langle \boldsymbol{e}_{jn}, \boldsymbol{h}_{j+1,m}\rangle_{S_j} \quad (n=1, 2, 3...), (2.10)$$

and at $z = 0$

$$\sum_m F_{Nm}\langle \boldsymbol{e}_{Nm}, \boldsymbol{h}_{N+1,n}\rangle_{S_N} = A_{N+1,n} \quad (n=1, 2, 3...)$$

$$D_{Nn} = \sum_m A_{N+1,m}\langle \boldsymbol{e}_{Nn}, \boldsymbol{h}_{N+1,m}\rangle_{S_N} \quad (n=1, 2, 3...) \quad (2.11)$$

where

$$D_{ir} \equiv A_{ir}\, e^{-\gamma_{ir}L_i} - B_{ir} \quad (2.12)$$

$$F_{ir} \equiv A_{ir}\, e^{-\gamma_{ir}L_i} + B_{ir}\,. \quad (2.13)$$

Truncating the infinite series to M_i modes in each ith region, equations (2.9)-(2.11) can be written in matrix form [19]:

at $z = -z_1$

$$\underline{\underline{G}}_1 (\underline{A}_1 + \underline{B}_1) = \underline{\underline{C}}_2 \underline{F}_2 + \underline{\underline{S}}_2 \underline{D}_2$$

$$\underline{A}_1 - \underline{B}_1 = \underline{\underline{G}}_1^T (\underline{\underline{C}}_2 \underline{D}_2 + \underline{\underline{S}}_2 \underline{F}_2), \quad (2.14)$$

at $z = -z_j$ $(j \neq 1, N)$

$$\underline{\underline{G}}_j \underline{F}_j = \underline{\underline{C}}_{j+1} \underline{F}_{j+1} + \underline{\underline{S}}_{j+1} \underline{D}_{j+1}$$

$$\underline{D}_j = \underline{\underline{G}}_j^T \left(\underline{\underline{C}}_{j+1} \underline{D}_{j+1} + \underline{\underline{S}}_{j+1} \underline{F}_{j+1} \right), \tag{2.15}$$

and at $z = 0$

$$\underline{\underline{G}}_N \underline{F}_N = \underline{A}_{N+1}$$

$$\underline{D}_N = \underline{\underline{G}}_N^T \underline{A}_{N+1} \tag{2.16}$$

where the T superscript indicates matrix transpose, $\underline{A}_1$ is the known incident modal coefficient column matrix of M_1 elements, $\underline{B}_1$ and $\underline{A}_{N+1}$ are the column matrices of M_1 and M_{N+1} elements of the unknown modal coefficients for the fields reflected in region 1 and transmitted in region N+1, respectively, and

$$\underline{D}_i = \left[A_{im} e^{-\gamma_{im} L_i} - B_{im} \right]_{M_i \text{ x } 1} \tag{2.17}$$

$$\underline{F}_i = \left[A_{im} e^{-\gamma_{im} L_i} + B_{im} \right]_{M_i \text{ x } 1} \tag{2.18}$$

$$\underline{\underline{C}}_i = \left[\delta_{mn} \cosh(\gamma_{im} L_i) \right]_{M_i \text{ x } M_i} \tag{2.19}$$

$$\underline{\underline{S}}_i = \left[\delta_{mn} \sinh(\gamma_{im} L_i) \right]_{M_i \text{ x } M_i} \tag{2.20}$$

$$\underline{\underline{G}}_i = \left[\langle \boldsymbol{e}_{im}, \boldsymbol{h}_{i+1,n} \rangle_{S_i} \right]_{M_{i+1} \text{ x } M_i}. \tag{2.21}$$

2.3.2 Boundary Reduction Discontinuities

For the boundary reduction case, at each discontinuity we take the vector product of the terms in the electric field continuity equation with a magnetic mode function from the preceding waveguide section, and the vector product of the terms in the magnetic field continuity equation with an electric mode function from the following waveguide section.

Applying the orthogonality of the modes, equations (2.5)-(2.7) become:

at $z = -z_1$

$$A_{1n} + B_{1n} = \sum_m \left(F_{2m} \cosh(\gamma_{2m} L_2) + D_{2m} \sinh(\gamma_{2m} L_2)\right) \langle \boldsymbol{e}_{2m}, \boldsymbol{h}_{1n} \rangle_{S_2} \quad (n = 1, 2, 3...)$$

$$\sum_m \left(A_{1m} - B_{1m}\right) \langle \boldsymbol{e}_{2n}, \boldsymbol{h}_{1m} \rangle_{S_2} = D_{2n} \cosh(\gamma_{2n} L_2) + F_{2n} \sinh(\gamma_{2n} L_2) \quad (n = 1, 2, 3...), \quad (2.22)$$

at $z = -z_j$ $(j \neq 1, N)$

$$F_{jn} = \sum_m \left(F_{j+1,m} \cosh(\gamma_{j+1,m} L_{j+1}) + D_{j+1,m} \sinh(\gamma_{j+1,m} L_{j+1})\right) \langle \boldsymbol{e}_{j+1,m}, \boldsymbol{h}_{jn} \rangle_{S_{j+1}} \quad (n = 1, 2, 3...)$$

$$\sum_m D_{jm} \langle \boldsymbol{e}_{j+1,n}, \boldsymbol{h}_{jm} \rangle_{S_{j+1}} = D_{j+1,n} \cosh(\gamma_{j+1,n} L_{j+1}) + F_{j+1,n} \sinh(\gamma_{j+1,n} L_{j+1}) \quad (n = 1, 2, 3...), (2.23)$$

and at $z = 0$

$$F_{Nn} = \sum_m A_{Nm} \langle \boldsymbol{e}_{N+1,m}, \boldsymbol{h}_{Nn} \rangle_{S_{N+1}} \quad (n = 1, 2, 3...)$$

$$\sum_m D_{Nm} \langle \boldsymbol{e}_{N+1,n}, \boldsymbol{h}_{Nm} \rangle_{S_{N+1}} = A_{N+1,n} \quad (n = 1, 2, 3...) \quad (2.24)$$

where D_{ir} and F_{ir} are defined in (2.12) and (2.13), respectively.

As before, the infinite series are truncated to M_i modes in each ith region. Equations (2.22)-(2.24) can be written in matrix form:

at $z = -z_1$

$$\underline{A}_1 + \underline{B}_1 = \underline{\underline{G}}_1^T \left(\underline{\underline{C}}_2 \underline{F}_2 + \underline{\underline{S}}_2 \underline{D}_2 \right)$$

$$\underline{\underline{G}}_1 \left(\underline{A}_1 - \underline{B}_1 \right) = \underline{\underline{C}}_2 \underline{D}_2 + \underline{\underline{S}}_2 \underline{F}_2, \quad (2.25)$$

at $z = -z_j$ $(j \neq 1, N)$

$$\underline{F}_j = \underline{\underline{G}}_j^T \left(\underline{\underline{C}}_{j+1} \underline{F}_{j+1} + \underline{\underline{S}}_{j+1} \underline{D}_{j+1} \right)$$

$$\underline{\underline{G}}_j \underline{D}_j = \underline{\underline{C}}_{j+1} \underline{D}_{j+1} + \underline{\underline{S}}_{j+1} \underline{F}_{j+1}, \tag{2.26}$$

and at $z = 0$

$$\underline{F}_N = \underline{\underline{G}}_N^T \underline{A}_{N+1}$$

$$\underline{\underline{G}}_N \underline{D}_N = \underline{A}_{N+1} \tag{2.27}$$

where the quantities are described in (2.17)-(2.20), except in the boundary reduction case

$$\underline{\underline{G}}_i = \left[\langle \boldsymbol{e}_{i+1,n}, \boldsymbol{h}_{im} \rangle_{S_{i+1}} \right]_{M_{i+1} \times M_i}. \tag{2.28}$$

The sets of linear matrix equations for an arbitrary combination of boundary enlargement and reduction discontinuities can be compiled by considering the corresponding matrix equations in (2.14)-(2.16) or (2.25)-(2.27).

2.4 Scattering Matrix Formulation

In scattering matrix formulation, $\underline{B}_1$ and $\underline{A}_{N+1}$ can be expressed as

$$\underline{B}_1 = \underline{\underline{S}}_{11} \underline{A}_1$$

$$\underline{A}_{N+1} = \underline{\underline{S}}_{21} \underline{A}_1 \tag{2.29}$$

where $\underline{\underline{S}}_{11}$ and $\underline{\underline{S}}_{21}$ are the complex reflection and transmission matrices for the entire structure, respectively. Solving the sets of linear matrix equations for an arbitrary series of boundary enlargement and reduction discontinuities, the scattering matrices are obtained as [20], [21]

$$\underline{\underline{S}}_{11} = \begin{cases} \underline{\underline{I}} - 2\,\underline{\underline{G}}_1^T\,\underline{\underline{Q}}_2\,\underline{\underline{U}}^{-1}\underline{\underline{G}}_1, \text{ for a 1st discontinuity boundary enlargement (B.E.)} \\ \\ -\underline{\underline{I}} + 2\,\underline{\underline{G}}_1^T\,\underline{\underline{Q}}_2\,\underline{\underline{U}}^{-1}\underline{\underline{G}}_1, \text{ for a 1st discontinuity boundary reduction (B.R.)} \end{cases} \tag{2.30}$$

$$\underline{\underline{S}}_{21} = 2\left(\underline{\underline{G}}_N\underline{\underline{R}}_N^{-1}\right)\left(\underline{\underline{G}}_{N-1}\underline{\underline{R}}_{N-1}^{-1}\right)\ldots\left(\underline{\underline{G}}_3\underline{\underline{R}}_3^{-1}\right)\underline{\underline{G}}_2\,\underline{\underline{U}}^{-1}\underline{\underline{G}}_1 \tag{2.31}$$

where $\underline{\underline{G}}_i$ ($i = 1, \ldots, N$) is determined by (2.21) or (2.28) for the ith discontinuity B.E. or B.R. case, respectively, $\underline{\underline{I}}$ is the unit matrix and

$$\underline{\underline{U}} = \begin{cases} \left(\underline{\underline{C}}_2 + \underline{\underline{G}}_1\,\underline{\underline{G}}_1^T\,\underline{\underline{S}}_2\right) + \left(\underline{\underline{S}}_2 + \underline{\underline{G}}_1\,\underline{\underline{G}}_1^T\,\underline{\underline{C}}_2\right)\underline{\underline{G}}_2^T\,\underline{\underline{Q}}_3\,\underline{\underline{R}}_3^{-1}\,\underline{\underline{G}}_2, \text{ for the 1st and 2nd} \\ \qquad\qquad\qquad\qquad\qquad\qquad\qquad\qquad\qquad\qquad \text{discontinuities both B.E. or B.R.} \\ \left(\underline{\underline{S}}_2 + \underline{\underline{G}}_1\,\underline{\underline{G}}_1^T\,\underline{\underline{C}}_2\right) + \left(\underline{\underline{C}}_2 + \underline{\underline{G}}_1\,\underline{\underline{G}}_1^T\,\underline{\underline{S}}_2\right)\underline{\underline{G}}_2^T\,\underline{\underline{Q}}_3\,\underline{\underline{R}}_3^{-1}\,\underline{\underline{G}}_2, \text{ otherwise.} \end{cases} \tag{2.32}$$

$\underline{\underline{Q}}_i$ and $\underline{\underline{R}}_i$ are M_i x M_i matrices calculated from the following recurrence formulas:

$$\underline{\underline{Q}}_i = \begin{cases} \underline{\underline{S}}_i + \underline{\underline{C}}_i\,\underline{\underline{G}}_i^T\,\underline{\underline{Q}}_{i+1}\,\underline{\underline{R}}_{i+1}^{-1}\,\underline{\underline{G}}_i, \text{ for the } i\text{th and } i\text{+1th discontinuities both B.E. or B.R.} \\ \\ \underline{\underline{C}}_i + \underline{\underline{S}}_i\,\underline{\underline{G}}_i^T\,\underline{\underline{Q}}_{i+1}\,\underline{\underline{R}}_{i+1}^{-1}\,\underline{\underline{G}}_i, \text{ otherwise} \end{cases} \tag{2.33}$$

$$\underline{\underline{R}}_i = \begin{cases} \underline{\underline{C}}_i + \underline{\underline{S}}_i\,\underline{\underline{G}}_i^T\,\underline{\underline{Q}}_{i+1}\,\underline{\underline{R}}_{i+1}^{-1}\,\underline{\underline{G}}_i, \text{ for the } i\text{th and } i\text{+1th discontinuities both B.E. or B.R.} \\ \\ \underline{\underline{S}}_i + \underline{\underline{C}}_i\,\underline{\underline{G}}_i^T\,\underline{\underline{Q}}_{i+1}\,\underline{\underline{R}}_{i+1}^{-1}\,\underline{\underline{G}}_i, \text{ otherwise} \end{cases} \tag{2.34}$$

with

$$\underline{\underline{Q}}_{N+1} \equiv \underline{\underline{R}}_{N+1} \equiv \underline{\underline{I}}. \tag{2.35}$$

The recurrence formulas, (2.33) and (2.34), require that the calculation of the scattering matrices begins at the Nth discontinuity and move successively to the 1st discontinuity.

2.5 SYMMETRIC DISCONTINUITIES

A longitudinally symmetric structure with N discontinuities can be reduced to N' discontinuities with $N'+1$ waveguide regions, $N' = N/2$, alternately terminated with a magnetic or electric wall. The magnetic and electric walls, placed at the symmetry plane bisecting the N discontinuity structure, correspond to the the even and odd mode excitation cases, respectively [11], [22].

If the N'th discontinuity and the symmetry plane are located at $z = 0$ and $z = L_{N'+1}/2$, respectively, then the electric and magnetic fields in the $N'+1$th region are as follows [11]:

$$\boldsymbol{E}_{t,N'+1} = \sum_m A_{N'+1,m}\left(e^{-\gamma_{N'+1,m}\, z} + \Gamma e^{\gamma_{N'+1,m}\,(z - L_{N'+1})}\right)\boldsymbol{e}_{N'+1,m}$$

$$\boldsymbol{H}_{t,N'+1} = \sum_m A_{N'+1,m}\left(e^{-\gamma_{N'+1,m}\, z} - \Gamma e^{\gamma_{N'+1,m}\,(z - L_{N'+1})}\right)\boldsymbol{h}_{N'+1,m} \qquad (2.36)$$

where $\Gamma = +1$ in the case of a magnetic wall (even excitation) and $\Gamma = -1$ in the case of an electric wall (odd excitation).

Let $\underline{\underline{S}}^e_{11}$ and $\underline{\underline{S}}^o_{11}$ be the reflection coefficient matrices of the N' discontinuities due to even and odd excitation, respectively. The scattering matrices for the original structure of N discontinuities can be calculated by superimposing the two cases [11]:

$$\underline{\underline{S}}_{11} = \frac{1}{2}\left(\underline{\underline{S}}^e_{11} + \underline{\underline{S}}^o_{11}\right)$$

$$\underline{\underline{S}}_{21} = \frac{1}{2}\left(\underline{\underline{S}}^e_{11} - \underline{\underline{S}}^o_{11}\right). \qquad (2.37)$$

$\underline{\underline{S}}^e_{11}$ and $\underline{\underline{S}}^o_{11}$ can be calculated using equation (2.30) where $\underline{\underline{Q}}_{N'+1}$ and $\underline{\underline{R}}_{N'+1}$ are as follows:

i) for a N'th discontinuity boundary enlargement

$$\underline{\underline{Q}}_{N'+1} = \begin{cases} \underline{\underline{T}}, \text{ even excitation} \\ \\ \underline{\underline{I}}, \text{ odd excitation} \end{cases} \qquad (2.38a)$$

$$\underline{\underline{R}}_{N'+1} = \begin{cases} \underline{\underline{I}}, \text{ even excitation} \\ \\ \underline{\underline{T}}^{-1}, \text{ odd excitation} \end{cases} \tag{2.38b}$$

ii) for a N'th discontinuity boundary reduction

$$\underline{\underline{Q}}_{N'+1} = \begin{cases} \underline{\underline{I}}, \text{ even excitation} \\ \\ \underline{\underline{T}}, \text{ odd excitation} \end{cases} \tag{2.39a}$$

$$\underline{\underline{R}}_{N'+1} = \begin{cases} \underline{\underline{T}}^{-1}, \text{ even excitation} \\ \\ \underline{\underline{I}}, \text{ odd excitation} \end{cases} \tag{2.39b}$$

where

$$\underline{\underline{T}} = [\ \delta_{mn} \tanh(\gamma_{N'+1,m} L_{N'+1}/2)\ ]_{M_{N'+1} \times M_{N'+1}} . \tag{2.40}$$

The computational advantage of using the even and odd excitation in the analysis is apparent from the number of full complex matrix inversions required. Calculating $\underline{\underline{S}}^{e}_{11}$ and $\underline{\underline{S}}^{o}_{11}$ each require $N'-1$ matrix inversions of size $M_i \times M_i$ ($i = 2, \ldots, N'$) for a total of $N-2$ matrix inversions. If calculated as in the previous section, the same N discontinuities would require $N-1$ matrix inversions of size $M_i \times M_i$ ($i = 2, \ldots, N$). The computational effort is therefore reduced by one $M_N \times M_N$ complex matrix inversion when the symmetry is used in the analysis.

CHAPTER 3

APPLICATION TO CIRCULAR WAVEGUIDES

In this chapter, the general scattering formulation presented in Chapter 2 is applied to circular waveguide discontinuities for numerical computations. Closed form expressions for the vector products used in (2.21) and (2.28) are derived for circular waveguides.

3.1 Modal Function Expressions

The fields in a circular cylindrical waveguide can be expressed as a combination of TE and TM components. Assuming an $e^{j\omega t}$ time dependence, the components of the transverse electric and magnetic fields can be written in circular cylindrical coordinates (r, ϕ, z) [22]

$$E_r = -\gamma\, k_c A_m J'_m(k_c r)\cos(m\phi) - j\omega\mu \frac{m}{r} B_m J_m(k_c r)\cos(m\phi)$$

$$E_\phi = \gamma \frac{m}{r} A_m J_m(k_c r)\sin(m\phi) + j\omega\mu\, k_c B_m J'_m(k_c r)\sin(m\phi)$$

$$H_r = -j\omega\varepsilon \frac{m}{r} A_m J_m(k_c r)\sin(m\phi) - \gamma\, k_c B_m J'_m(k_c r)\sin(m\phi)$$

$$H_\phi = -j\omega\varepsilon\, k_c A_m J'_m(k_c r)\cos(m\phi) - \gamma \frac{m}{r} B_m J_m(k_c r)\cos(m\phi) \qquad (3.1)$$

where A_m and B_m are the amplitudes of the TM and TE components, respectively, ε and μ are the permittivity and permeability of the medium filling the waveguide, respectively, ω is the angular frequency, γ is the propagation constant, $J_m(k_c r)$ is the Bessel function of the first kind of order m where the prime indicates differentiation with respect to the argument $k_c r$, and $k_c^2 = k^2 + \gamma^2$ where k is the wave number ($k = \omega\sqrt{\varepsilon\mu}$). The modal propagation constants can be calculated from the general characteristic equation derived in [23].

3.2 Modal Coupling Integrals

The coupling between the ith and jth mode over the cross section S is given by

$$\langle \boldsymbol{E}_{ti}, \boldsymbol{H}_{tj} \rangle_S = \int_S (\boldsymbol{E}_{ti} \times \boldsymbol{H}_{tj}) \cdot d\boldsymbol{s} = \int_0^{2\pi} \int_0^a (E_{ri} H_{\phi j} - E_{\phi i} H_{rj})\, r\, dr\, d\phi \qquad (3.2)$$

Substituting the expressions of the derivatives of the Bessel function, and simplifying gives for $i \neq j$

$$\langle \boldsymbol{E}_{ti}, \boldsymbol{H}_{tj} \rangle_S = \frac{\pi}{2} \frac{k_{ci}\, k_{cj}}{k_{ci} - k_{cj}} Y_j\, a \{ k_{ci} J_m(k_{ci}\, a) [\mathrm{F}_1 J_{m-1}(k_{cj}\, a) - \mathrm{F}_2 J_{m+1}(k_{cj}\, a)] - k_{cj} J_m(k_{cj}\, a) [\mathrm{F}_1 J_{m-1}(k_{ci}\, a) - \mathrm{F}_2 J_{m+1}(k_{ci}\, a)] \} \qquad (3.3)$$

where $Y = \sqrt{\varepsilon / \mu} = 1/Z$ and

$$\mathrm{F}_1 = \mathrm{j} k_j \gamma_i A_i A_j - k_i k_j Z_i B_i A_j + \gamma_i \gamma_j Z_j A_i B_j + \mathrm{j} k_i \gamma_j Z_i Z_j B_i B_j$$

$$\mathrm{F}_2 = \mathrm{j} k_j \gamma_i A_i A_j + k_i k_j Z_i B_i A_j - \gamma_i \gamma_j Z_j A_i B_j + \mathrm{j} k_i \gamma_j Z_i Z_j B_i B_j \qquad (3.4)$$

The transverse fields of the ith mode, $\boldsymbol{E}_{ti}$ and $\boldsymbol{H}_{ti}$, are normalized by dividing by $(\langle \boldsymbol{E}_{ti}, \boldsymbol{H}_{ti} \rangle_S)^{1/2}$ where S is the waveguide cross section of radius a

$$\langle \boldsymbol{E}_{ti}, \boldsymbol{H}_{ti} \rangle_S = \frac{\pi}{4} Y_i \{ (\mathrm{F}_1 + \mathrm{F}_2)(k_{ci}\, a)^2 [J_{m+1}^2(k_{ci}\, a) - J_m(k_{ci}\, a) J_{m+2}(k_{ci}\, a)] - 4m \mathrm{F}_2 J_m^2(k_{ci}\, a) \} \qquad (3.5)$$

The fields, (3.1), will not be a combination of TE and TM modes for the special case of a perfectly conducting waveguide. The mode amplitudes for the ith mode in (3.1) and (3.4) are then $A_i = 0$ and $B_i = 1$, and $A_i = 1$ and $B_i = 0$ for the TE and TM cases, respectively. The eigenvalues of the ith mode in a waveguide of radius a, $k_{ci}\, a$, are the roots of the Bessel function and the roots of the first derivative of the Bessel function for the TM and TE cases, respectively. Equations (3.3) and (3.5) can be further simplified for the TE-TE, TE-TM, TM-TE, and TM-TM region i - region j mode coupling cases; however, this would result in a total of ten equations for both the boundary enlargement and reduction cases whereas (3.3) and (3.5) cover all the cases. It should be noted that equation (3.3) equals zero for the TM-TE mode coupling case.

For a waveguide structure with an incident TE_{11} mode ($m = 1$), only the TE_{1n} and TM_{1n} modes will be excited at the discontinuities.

3.3 NUMERICAL RESULTS

The formulation is applied to a thick iris to study the convergence and to verify the accuracy of the analytic expressions. Also, application is made to the design of iris matched dielectric windows.

3.3.1 Convergence and Accuracy

Consider a thick circular iris of radius b and length L in a circular waveguide of radius a, as shown in Fig. 3.1. The iris forms a double discontinuity comprised of a boundary reduction followed by a boundary enlargement at a distance L.

The optimum ratio of the number of modes should be $M/N \approx a/b$, with $M = P$, where M, N, and P are the number of modes in regions 1, 2, and 3, respectively [6], [7], [24]. Choosing the number of modes according to this ratio should ensure fast and accurate results. This is illustrated here by studying the numerical results for an incident TE_{11} mode.

In Fig. 3.2 and Fig. 3.3, the magnitude of the reflection coefficient is shown as a function of P for fixed M and N, and as a function of M ($P = M$) for fixed N, respectively. It is observed that the reflection coefficient remains essentially constant after $P = M$ in Fig. 3.2, and after $M/N = a/b$ in Fig. 3.3. This indicates that the predicted optimum ratio of modes represents a critical value needed for accurate results.

The convergence of the magnitude of the reflection coefficient with different ratios of M/N ($P = M$ from now on) is shown in Fig. 3.4 through Fig. 3.6 for several values of L/a and ka. It is clear that the solution converges for all ratios of M/N, but the convergence is always fastest when $M/N = a/b$. Also, the rate of convergence is observed to be slower as the frequency increases and less dependent on the ratio of modes as the distance between the discontinuities L increases.

The reflection and transmission coefficients for decreasing values of L/a are shown in Table 3.1 and Table 3.2, respectively, where $M = N(a/b) = 40$. It is observed that the ratio M/N has a noticeable effect on the solution as L/a decreases. In the case of an infinitely

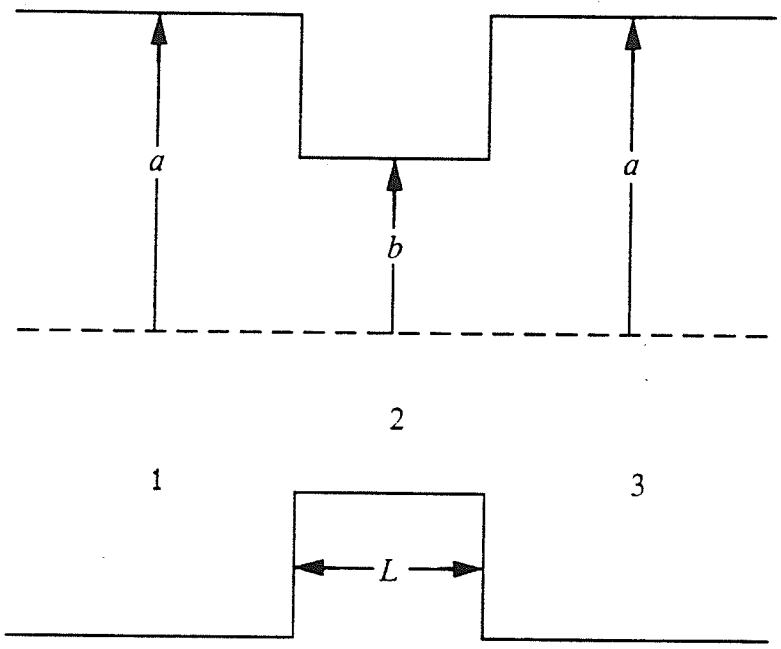

Fig. 3.1. Geometry of a thick iris.

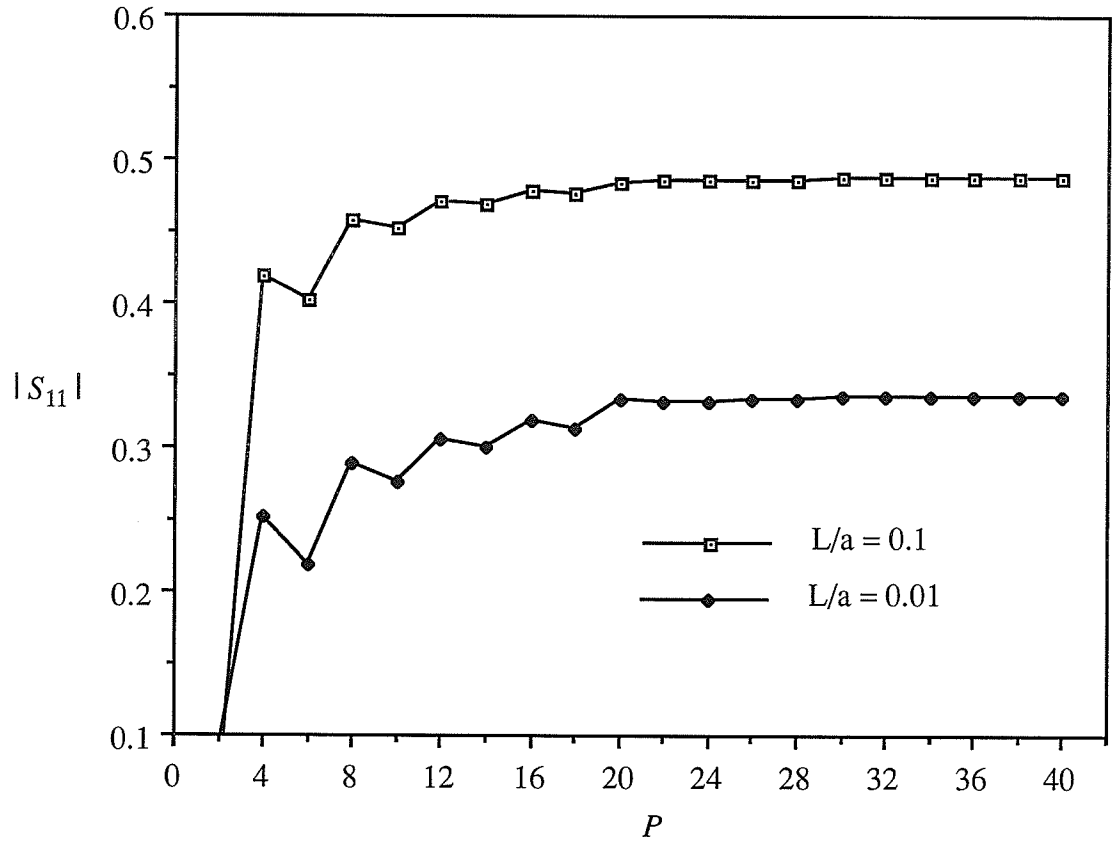

Fig. 3.2. Magnitude of the reflection coefficient as a function of P with $M = N(a/b) = 20$, for a thick iris with $a = 2b$ and $ka = 3.2$.

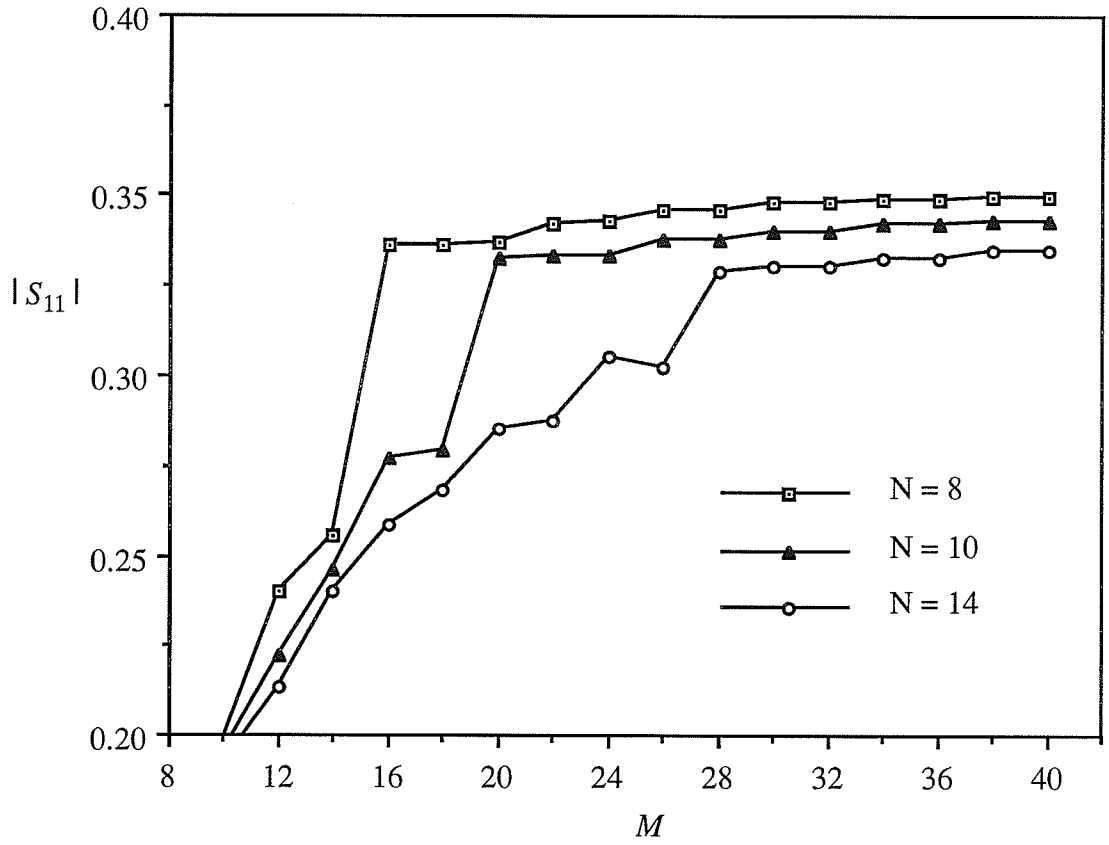

Fig. 3.3. Magnitude of the reflection coefficient as a function of M ($P = M$) for a thick iris with $a = 2b$, $L/a = 0.01$, and $ka = 3.2$.

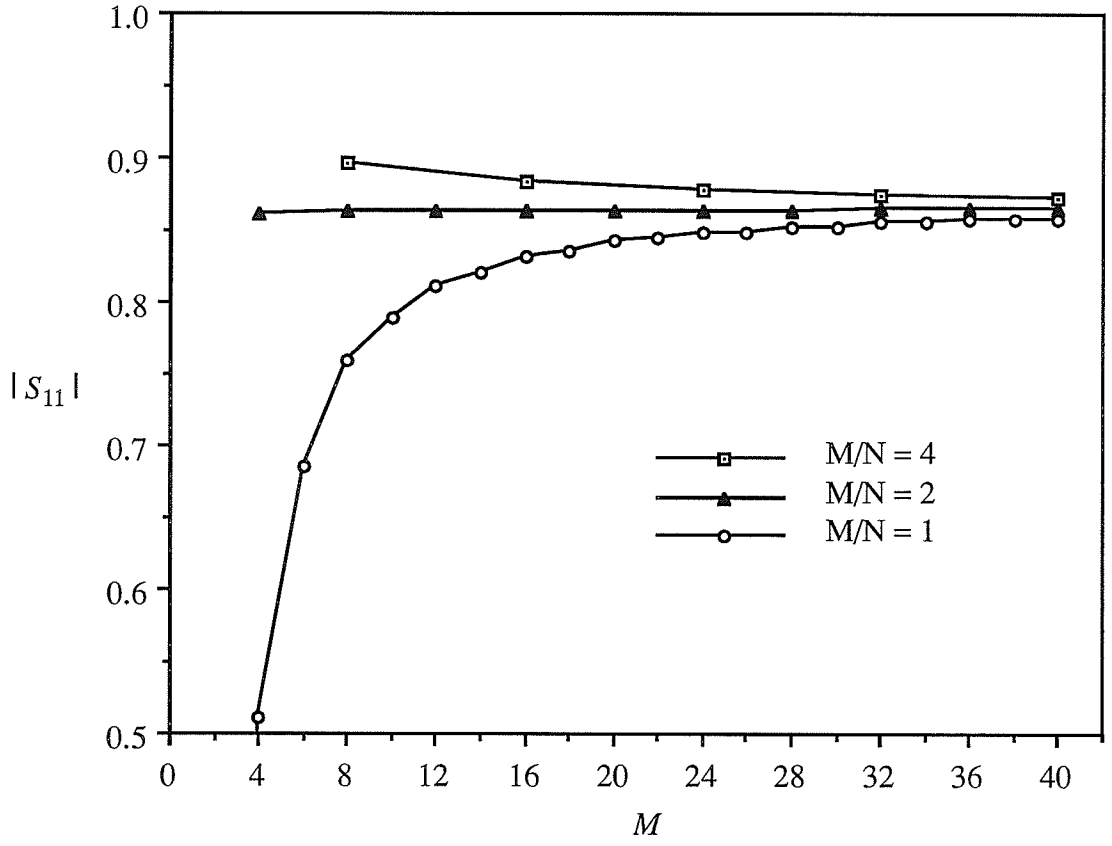

Fig. 3.4. Convergence of the magnitude of the reflection coefficient as a function of M for a thick iris with $a = 2b$, $L/a = 0.01$, and $ka = 2.4$.

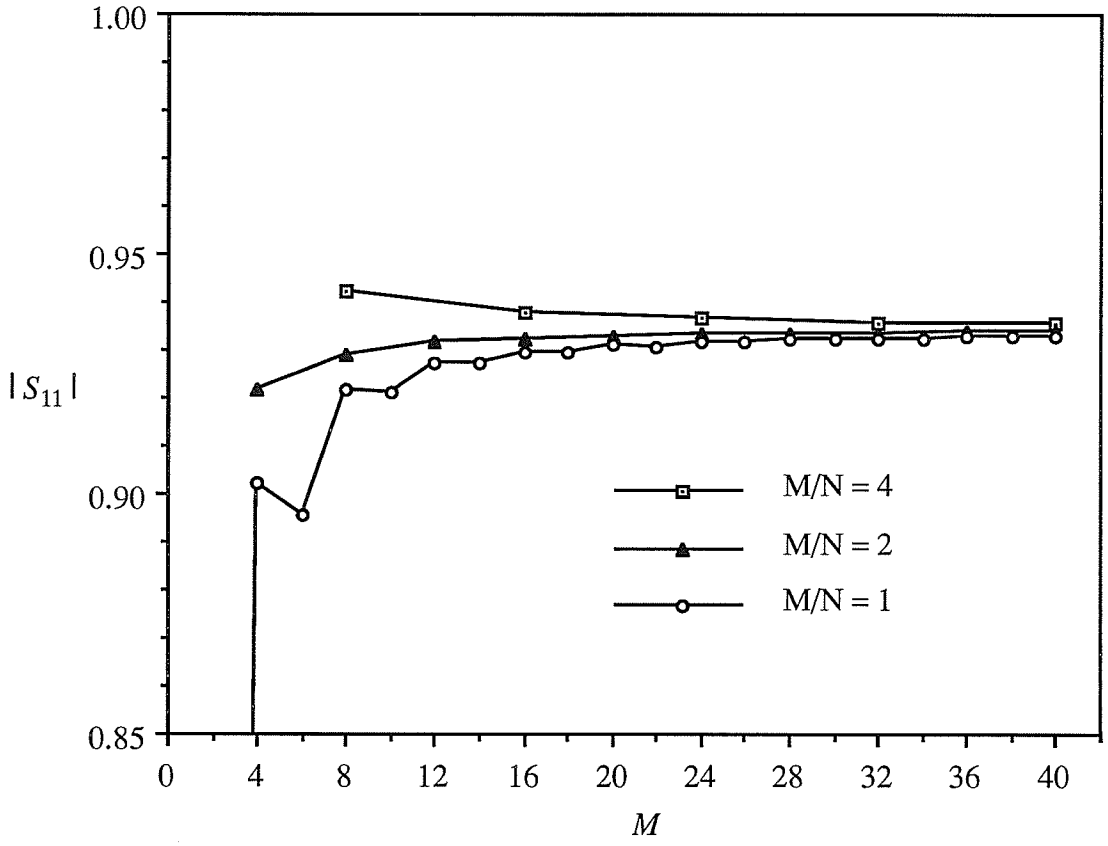

Fig. 3.5. Convergence of the magnitude of the reflection coefficient as a function of M for a thick iris with $a = 2b$, $L/a = 0.1$, and $ka = 2.4$.

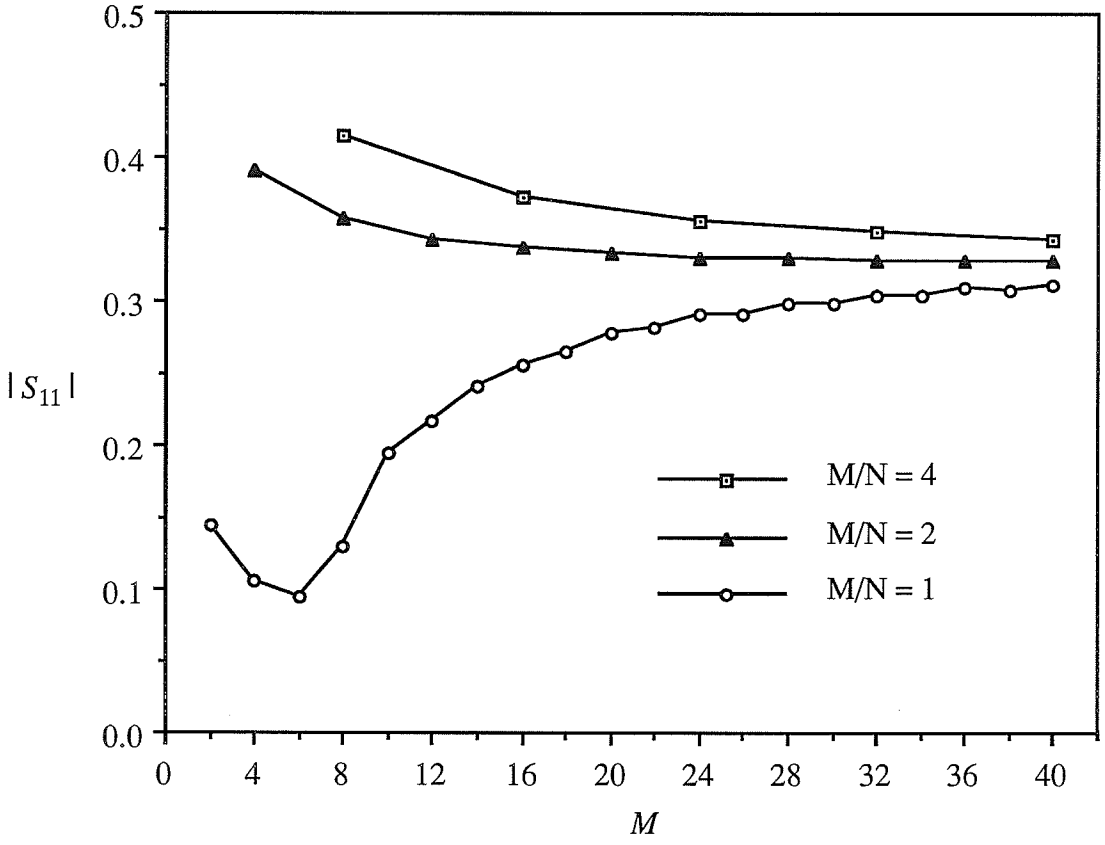

Fig. 3.6. Convergence of the magnitude of the reflection coefficient as a function of M for a thick iris with $a = 2b$, $L/a = 0.01$, and $ka = 3.2$.

Table 3.1

Reflection coefficient as a function of L/a for a thick iris with $a = 2b$ and $ka = 3.2$.

L/a	$M/N = a/b$	$M/N = 1$
10^{-1}	–0.18947 + j0.44710	–0.18518 + j0.44395
10^{-2}	–0.10399 + j0.31072	–0.09394 + j0.29725
10^{-3}	–0.09509 + j0.29387	–0.06417 + j0.24557
10^{-4}	–0.09433 + j0.29232	–0.05024 + j0.21846
10^{-5}	–0.09425 + j0.29173	–0.03272 + j0.17789
10^{-6}	–0.09424 + j0.29215	–0.02935 + j0.16878
0.0	–0.09424 + j0.29215	0.00000 + j0.00000

Table 3.2

Transmission coefficient as a function of L/a for a thick iris with $a = 2b$ and $ka = 3.2$.

L/a	$M/N = a/b$	$M/N = 1$
10^{-1}	0.80490 + j0.34110	0.80914 + j0.33751
10^{-2}	0.89596 + j0.29982	0.90601 + j0.28628
10^{-3}	0.90492 + j0.29278	0.93584 + j0.24448
10^{-4}	0.90568 + j0.29222	0.94977 + j0.21836
10^{-5}	0.90575 + j0.29217	0.96729 + j0.17787
10^{-6}	0.90576 + j0.29216	0.97065 + j0.16878
0.0	0.90576 + j0.29216	1.00000 + j0.00000

thin iris, the formulation mathematically collapses for $M/N = 1$ in the sense that (2.30) and (2.31) become zero and unit matrices, respectively. The numerical results always converge to the correct solution when $M/N = a/b$ as a result of the linear system being well conditioned [7].

To verify the accuracy of the formulation, comparison with numerical results calculated by the moment method [14] are shown in Table 3.3 through Table 3.10. For L less than 0.2 inches, excellent agreement of results are achieved with $M = N(a/b) = 40$. However, as L increases the number of modes must be reduced to avoid numerical instabilities as $\underline{\underline{U}}$ becomes too ill-conditioned for inversion. Significant disagreement, particularly in the phase, is observed for large L as the frequency increases and the ratio a/b decreases. In Table 3.4, Table 3.6, and Table 3.8, the magnitude of the transmission coefficient decreases to zero as L increases due to the iris region being below cutoff at the operating frequency. The proposed formulation requires the inversion of one N x N matrix, with N shown in the tables, while two 40 x 40 matrix inversions are needed in [14].

The numerical difficulties with the matrix inversions arise from the effect of the hyperbolic functions in (2.19) and (2.20). As the separation distance between a discontinuity increases, the highest order modes, which are below cutoff, cause the hyperbolic functions to become excessively large in that region. As a result, the matrices (2.32) and (2.34) may be too ill-conditioned for inversion. Reducing the number of modes used alleviates the problem by omitting the troublesome higher order modes, but the accuracy of the solution may suffer as already demonstrated. $\underline{\underline{R}}_i$ is more stable than $\underline{\underline{U}}$ since $\underline{\underline{R}}_i$ has fewer matrix terms with hyperbolic functions. For example, $\underline{\underline{R}}_i$ would be invertible in the iris regions specified in the tables when $L = 1.0$ inch and $M = N(a/b) = 40$, while $\underline{\underline{U}}$ is not invertible.

A modified formulation that restricts the higher order mode interaction between discontinuities for large distances between discontinuities, without compromising the accuracy, will be presented in Chapter 4.

Table 3.3

Comparison of the reflection coefficient as a function of L for a thick iris with $a = 0.50175$ in, $b = 0.25$ in, and $f = 9$ GHz.

L (inch)	Moment Method [14]		Proposed Formulation			
	Magnitude	Phase (degrees)	Magnitude	Phase (degrees)	M	N
0.005	0.867	149.8	0.864	149.4	40	20
0.008	0.874	150.4	0.872	150.1	40	20
0.050	0.934	155.7	0.934	155.6	40	20
0.100	0.966	158.6	0.965	158.5	40	20
0.200	0.990	161.0	0.989	160.9	20	10
0.500	1.000	162.0	0.999	161.7	12	6
1.000	1.000	162.0	1.000	161.8	4	2
3.000	1.000	162.0	1.000	151.9	2	1

Table 3.4

Comparison of the transmission coefficient as a function of L for a thick iris with $a = 0.50175$ in, $b = 0.25$ in, and $f = 9$ GHz.

L (inch)	Moment Method [14]		Proposed Formulation			
	Magnitude	Phase (degrees)	Magnitude	Phase (degrees)	M	N
0.005	0.498	59.8	0.503	59.4	40	20
0.008	0.485	60.4	0.489	60.1	40	20
0.050	0.356	65.7	0.358	65.6	40	20
0.100	0.260	68.6	0.261	68.5	40	20
0.200	0.144	71.0	0.145	70.9	20	10
0.500	0.027	72.0	0.027	71.8	12	6
1.000	0.002	72.0	0.002	71.8	4	2
3.000	0.000	75.7	0.000	61.9	2	1

Table 3.5

Comparison of the reflection coefficient as a function of L for a thick iris with $a = 0.50175$ in, $b = 0.25$ in, and $f = 12$ GHz.

L (inch)	Moment Method [14]		Proposed Formulation			
	Magnitude	Phase (degrees)	Magnitude	Phase (degrees)	M	N
0.005	0.331	108.7	0.328	108.5	40	20
0.008	0.344	109.1	0.340	108.9	40	20
0.050	0.488	113.2	0.486	113.0	40	20
0.100	0.622	116.8	0.620	116.6	40	20
0.200	0.806	122.0	0.803	121.8	20	10
0.500	0.977	127.4	0.976	126.9	8	4
1.000	0.999	128.1	1.000	126.9	4	2
3.000	1.000	128.2	1.000	68.5	2	1

Table 3.6

Comparison of the transmission coefficient as a function of L for a thick iris with $a = 0.50175$ in, $b = 0.25$ in, and $f = 12$ GHz.

L (inch)	Moment Method [14]		Proposed Formulation			
	Magnitude	Phase (degrees)	Magnitude	Phase (degrees)	M	N
0.005	0.943	18.7	0.945	18.5	40	20
0.008	0.939	19.1	0.940	18.9	40	20
0.050	0.873	23.2	0.874	23.0	40	20
0.100	0.783	26.8	0.784	26.6	40	20
0.200	0.593	32.0	0.596	31.8	20	10
0.500	0.211	37.4	0.217	36.9	8	4
1.000	0.034	38.1	0.038	36.9	4	2
3.000	0.000	38.1	0.000	–21.5	2	1

Table 3.7

Comparison of the reflection coefficient as a function of L for a thick iris with $a = 0.50175$ in, $b = 0.375$ in, and $f = 9$ GHz.

L (inch)	Moment Method [14]		Proposed Formulation			
	Magnitude	Phase (degrees)	Magnitude	Phase (degrees)	M	N
0.005	0.199	100.8	0.196	100.7	40	30
0.008	0.205	100.8	0.202	100.6	40	30
0.050	0.272	99.3	0.270	99.2	40	30
0.100	0.337	97.0	0.336	96.9	40	30
0.200	0.453	92.4	0.450	92.2	16	12
0.500	0.706	82.0	0.701	81.5	8	6
1.000	0.901	73.4	0.865	61.3	4	3
3.000	0.999	68.7	0.999	51.8	1	1

Table 3.8

Comparison of the transmission coefficient as a function of L for a thick iris with $a = 0.50175$ in, $b = 0.375$ in, and $f = 9$ GHz.

L (inch)	Moment Method [14]		Proposed Formulation			
	Magnitude	Phase (degrees)	Magnitude	Phase (degrees)	M	N
0.005	0.980	10.8	0.981	10.7	40	30
0.008	0.979	10.8	0.979	10.6	40	30
0.050	0.962	9.3	0.963	9.2	40	30
0.100	0.941	7.0	0.942	6.9	40	30
0.200	0.892	2.4	0.893	2.2	16	12
0.500	0.708	–8.0	0.713	–8.5	8	6
1.000	0.434	–16.6	0.486	–28.6	4	3
3.000	0.052	–21.3	0.063	–38.2	1	1

Table 3.9

Comparison of the reflection coefficient as a function of L for a thick iris with $a = 0.50175$ in, $b = 0.375$ in, and $f = 12$ GHz.

L (inch)	Moment Method [14]		Proposed Formulation			
	Magnitude	Phase (degrees)	Magnitude	Phase (degrees)	M	N
0.005	0.006	89.3	0.007	89.4	40	30
0.008	0.005	88.5	0.005	88.7	40	30
0.050	0.014	–102.2	0.014	–102.1	40	30
0.100	0.033	–114.4	0.033	–114.5	40	30
0.200	0.056	–138.6	0.056	–138.6	16	12
0.500	0.040	150.8	0.041	150.9	8	6
1.000	0.067	–146.3	0.067	–144.3	1	1
3.000	0.010	–74.6	0.025	107.6	1	1

Table 3.10

Comparison of the transmission coefficient as a function of L for a thick iris with $a = 0.50175$ in, $b = 0.375$ in, and $f = 12$ GHz.

L (inch)	Moment Method [14]		Proposed Formulation			
	Magnitude	Phase (degrees)	Magnitude	Phase (degrees)	M	N
0.005	1.000	–0.7	1.000	–0.7	40	30
0.008	1.000	–1.5	1.000	–1.5	40	30
0.050	1.000	–12.1	1.000	–12.1	40	30
0.100	0.999	–24.4	0.999	–24.4	40	30
0.200	0.998	–48.6	0.998	–48.6	16	12
0.500	0.999	–119.2	0.999	–119.2	8	6
1.000	0.998	123.7	0.998	125.8	1	1
3.000	1.000	15.4	1.000	17.6	1	1

3.3.2 Application to Iris Matched Dielectric Windows

Dielectric windows are used to isolate gas filled or vacuum regions in waveguides. The reflection coefficient of the dielectric window can be reduced by placing an iris on both sides of the window. Figure 3.7 shows an iris matched dielectric window in a circular waveguide of radius a where the dielectric window has relative permittivity ε_r and thickness L, and the irises have inner radius b and thickness L_i.

Design curves presented by Carin *et al.* [18] show the iris radius b that minimizes the reflection coefficient of an incident TE_{11} mode for a given a, ε_r, L, L_i, and operating frequency f. The reflection coefficient of the dielectric window was calculated by cascading the generalized scattering matrices of the four waveguide discontinuities. Ten modes were used for the field expansions in each waveguide region, but Fig. 3.4 and Fig. 3.6 in the previous section show that this may be inadequate number of modes to account for the higher mode interaction of closely spaced discontinuities. A better choice would be to use a higher number of modes in the ratio $M/N = a/b$ where M is the number of modes in the waveguide and dielectric regions and N is the number of modes in the iris regions.

To demonstrate the influence of the higher order modes, comparison with results calculated by the proposed formulation using $M = N(a/b) = 30$ is shown in Fig. 3.8. All dimensions are normalized to the waveguide radius a, and the frequency is normalized to the cutoff frequency f_c of the TE_{11} mode. The optimization was performed using the ZXGSN minimization routine from the International Mathematical and Statistical Library (IMSL) [25]. It is observed that the results for $L = 0.04a$ are within 1.2 percent, but an improvement of as much as 4.2 percent can be realized by increasing the number of modes for $L = 0.01a$. The frequency response of the matched window designs from Fig. 3.8 are shown in Fig. 3.9 through Fig. 3.12. Design curves for $L_i = 5L$ are shown in Fig. 3.13 with the corresponding frequency response curves shown in Fig. 3.14 through Fig. 3.17.

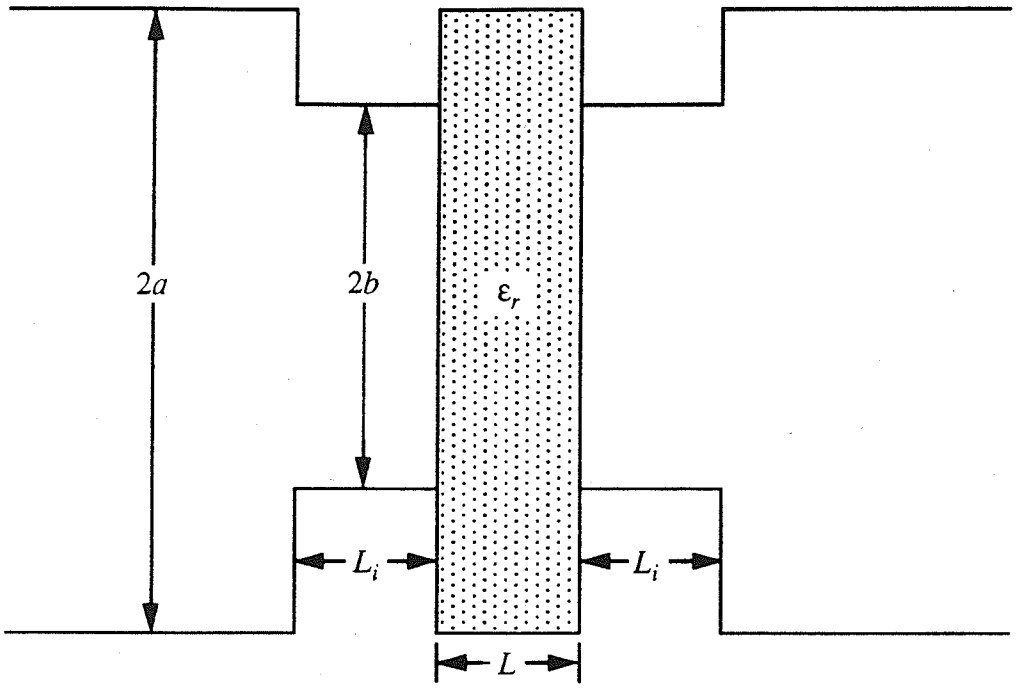

Fig. 3.7. Geometry of an iris matched dielectric window.

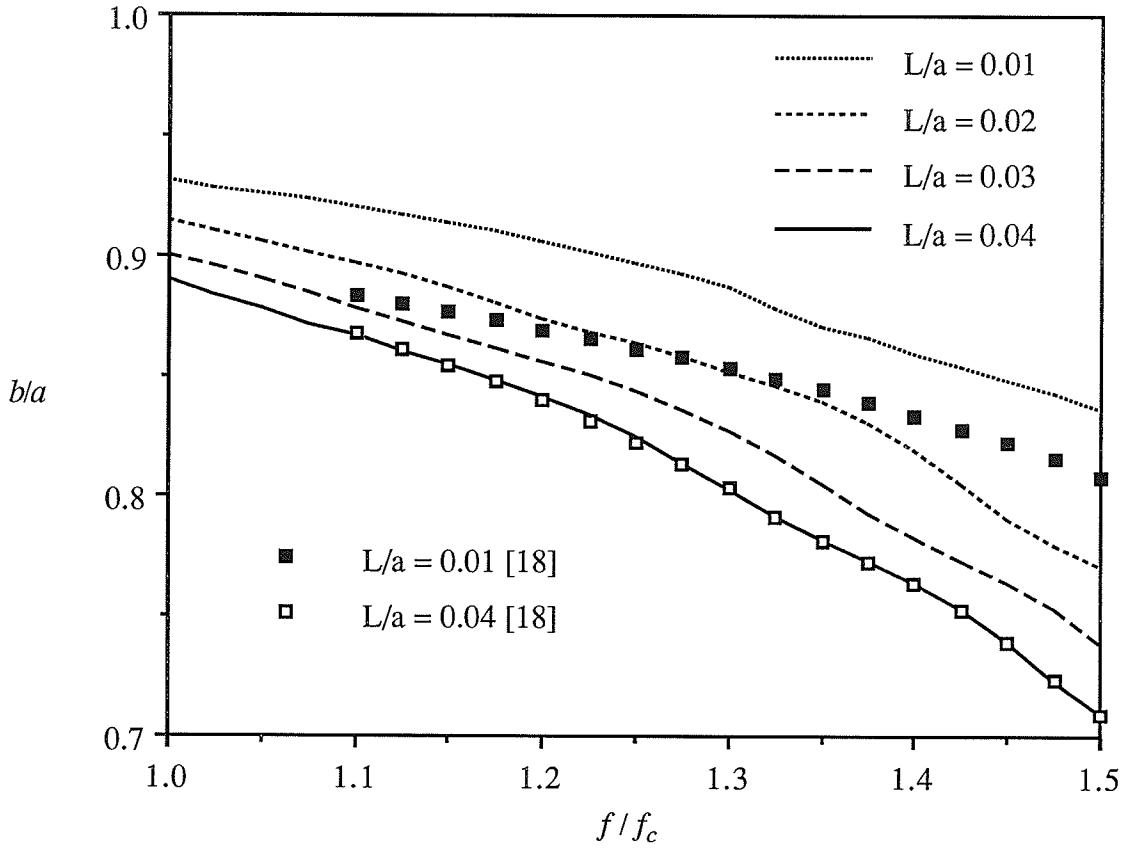

Fig. 3.8. Optimum iris radius as a function of the normalized frequency for an iris matched dielectric window with $\varepsilon_r = 2.8$ and $L_i = L$.

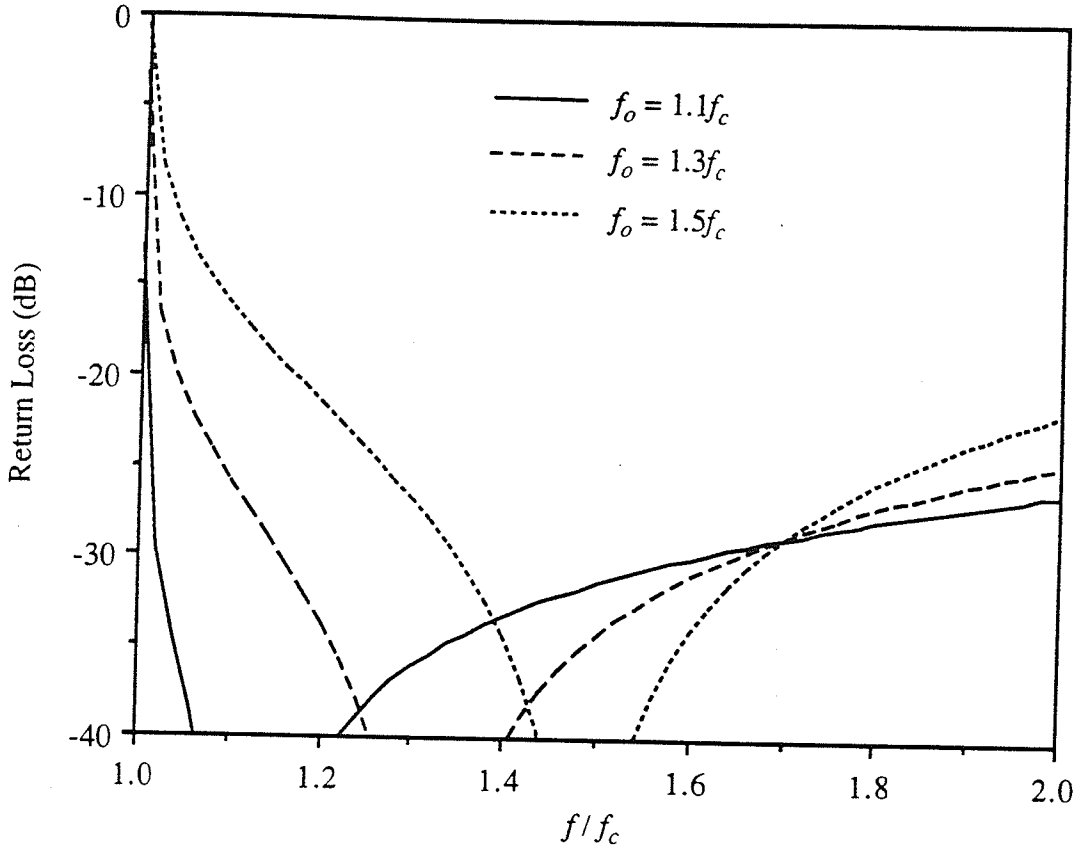

Fig. 3.9. Return loss as a function of normalized frequency for an iris matched dielectric window optimized for f_o / f_c = 1.1, 1.3, and 1.5 with ε_r = 2.8, L/a = 0.01, and $L_i = L$.

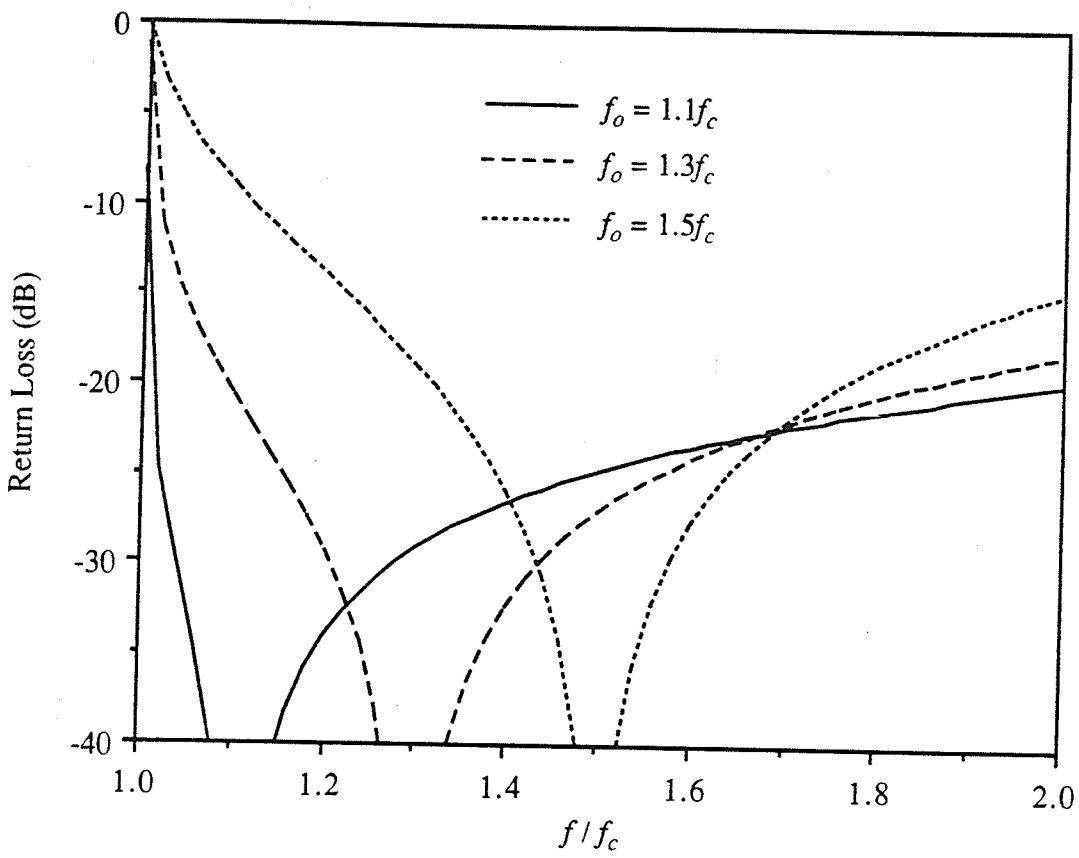

Fig. 3.10. Return loss as a function of normalized frequency for an iris matched dielectric window optimized for f_o / f_c = 1.1, 1.3, and 1.5 with ε_r = 2.8, L/a = 0.02, and $L_i = L$.

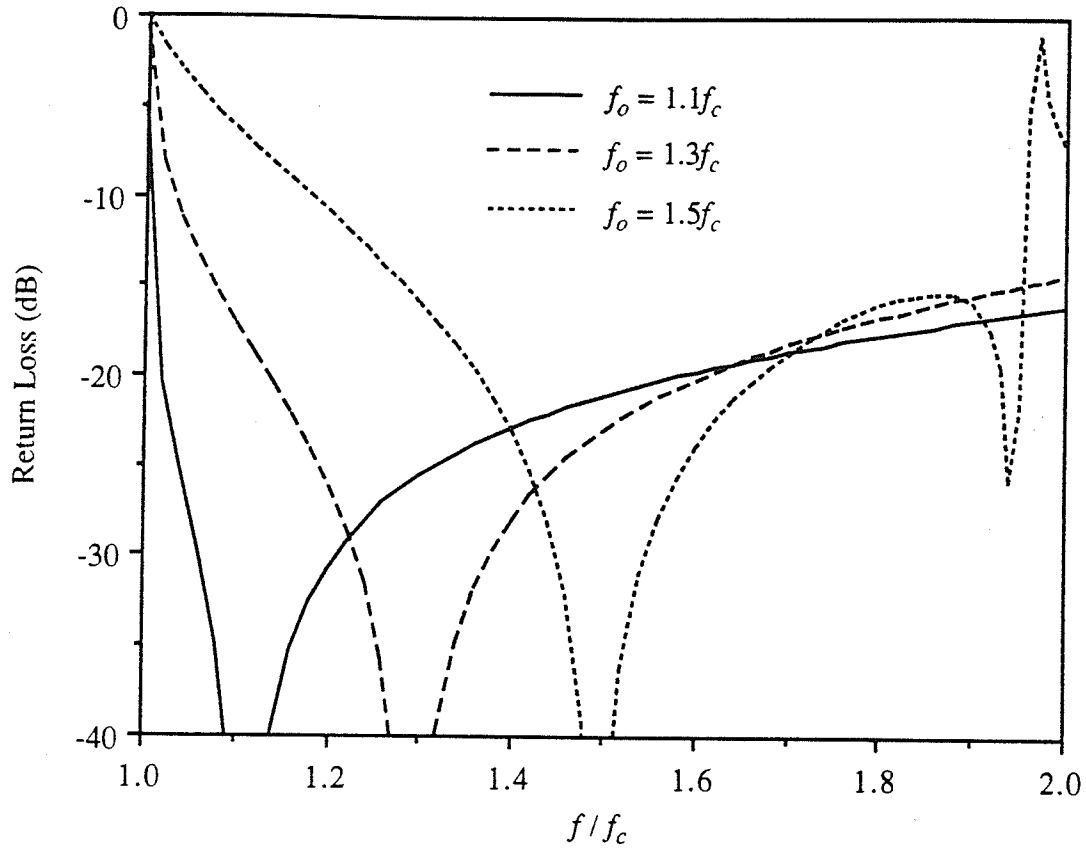

Fig. 3.11. Return loss as a function of normalized frequency for an iris matched dielectric window optimized for f_o / f_c = 1.1, 1.3, and 1.5 with ε_r = 2.8, L/a = 0.03, and $L_i = L$.

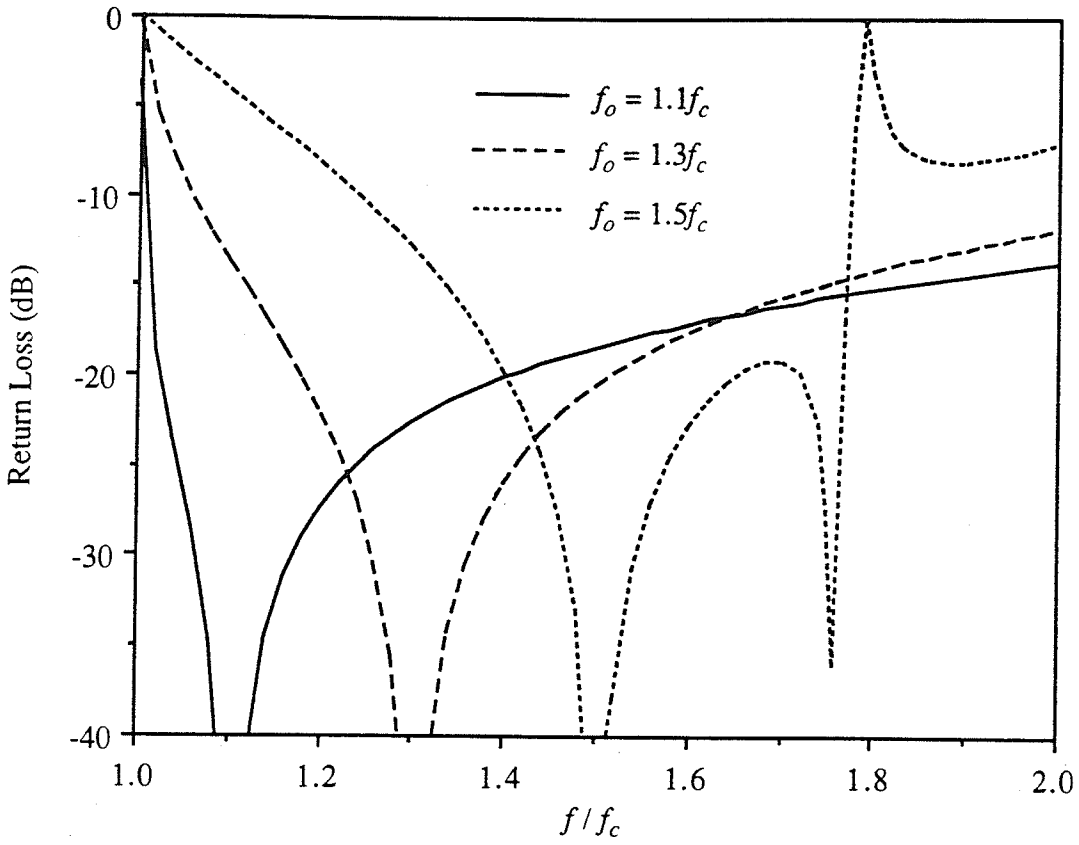

Fig. 3.12. Return loss as a function of normalized frequency for an iris matched dielectric window optimized for f_o / f_c = 1.1, 1.3, and 1.5 with ε_r = 2.8, L/a = 0.04, and $L_i = L$.

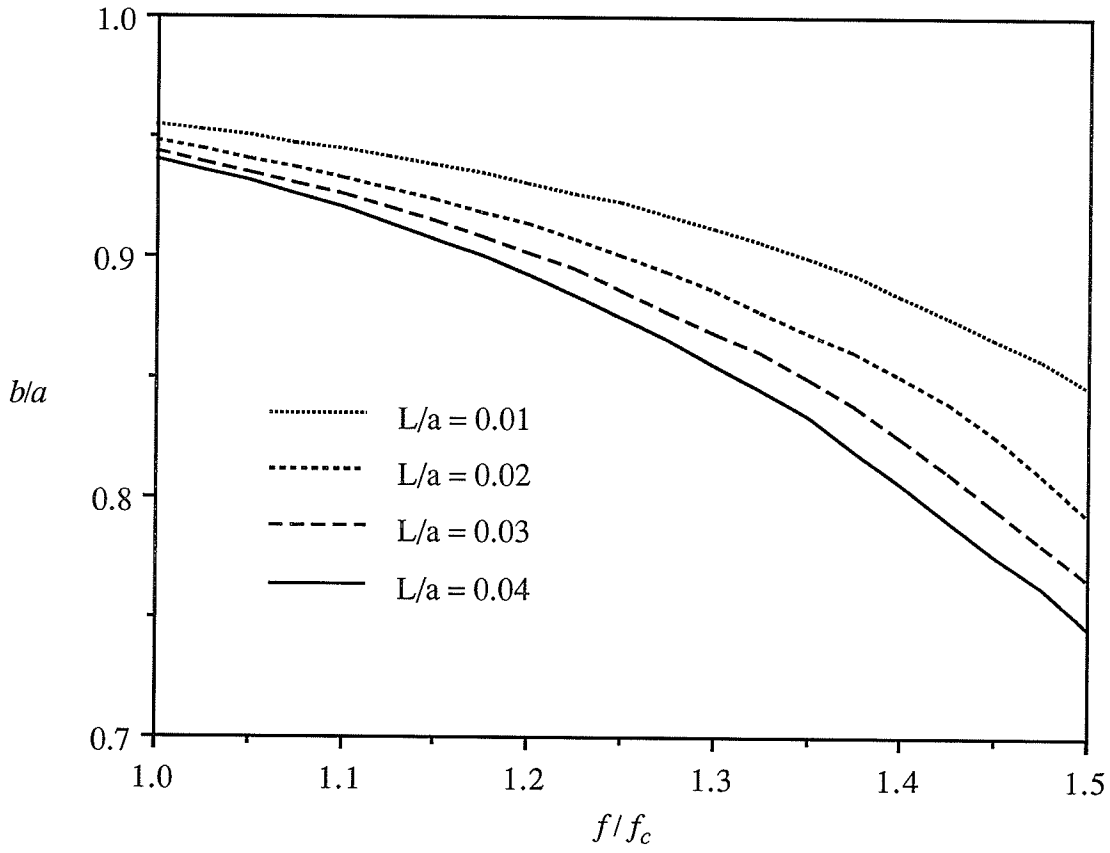

Fig. 3.13. Optimum iris radius as a function of the normalized frequency for an iris matched dielectric window with $\varepsilon_r = 2.8$ and $L_i = 5L$.

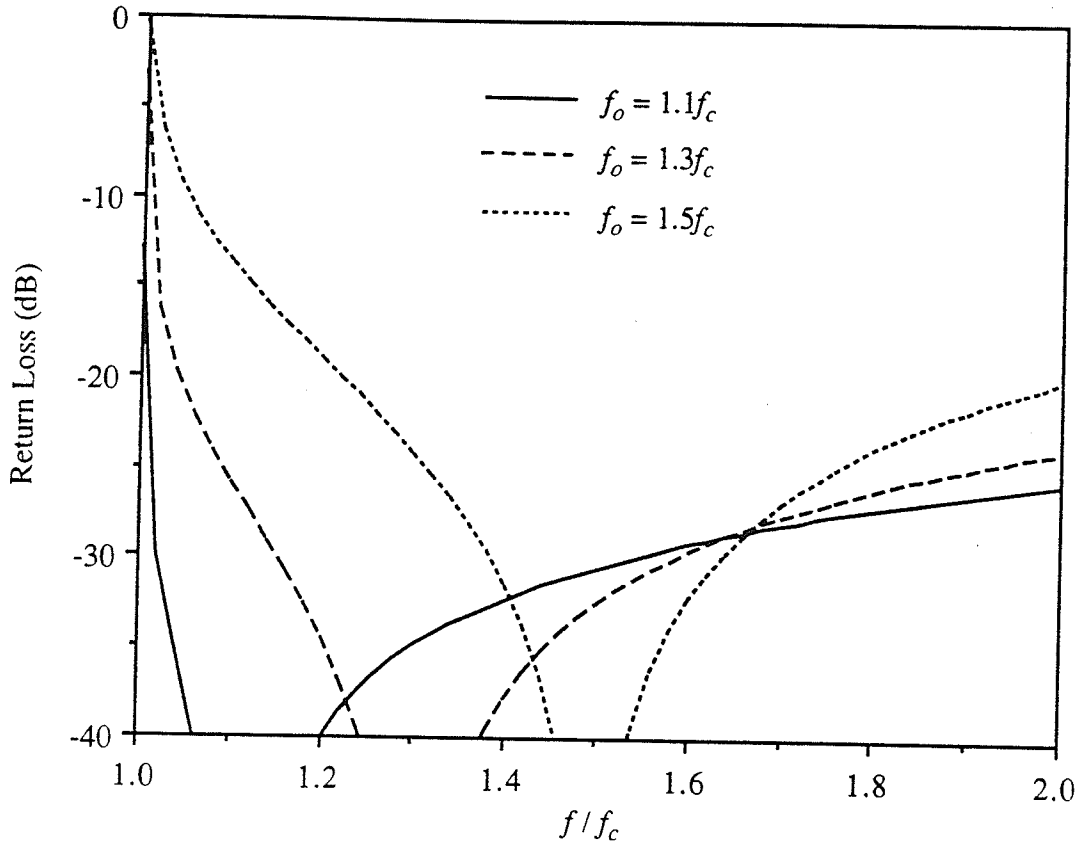

Fig. 3.14. Return loss as a function of normalized frequency for an iris matched dielectric window optimized for f_o / f_c = 1.1, 1.3, and 1.5 with ε_r = 2.8, L/a = 0.01, and $L_i = 5L$.

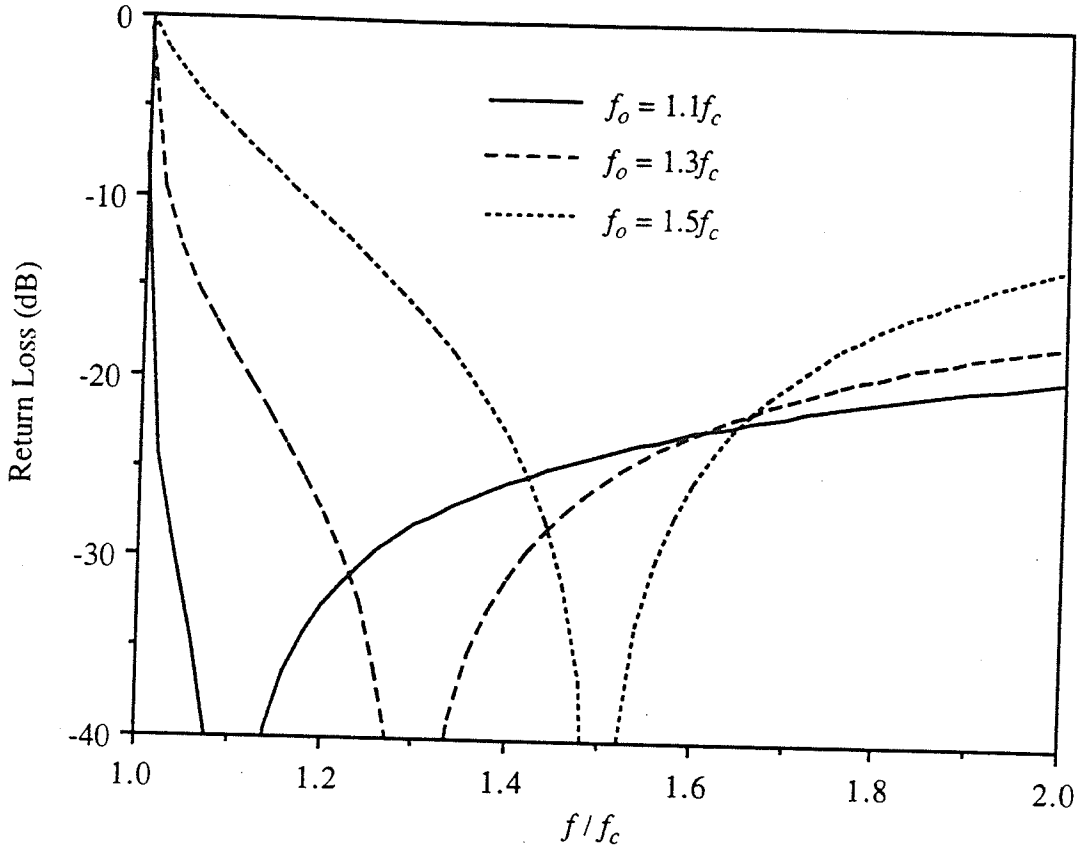

Fig. 3.15. Return loss as a function of normalized frequency for an iris matched dielectric window optimized for f_o / f_c = 1.1, 1.3, and 1.5 with ε_r = 2.8, L/a = 0.02, and $L_i = 5L$.

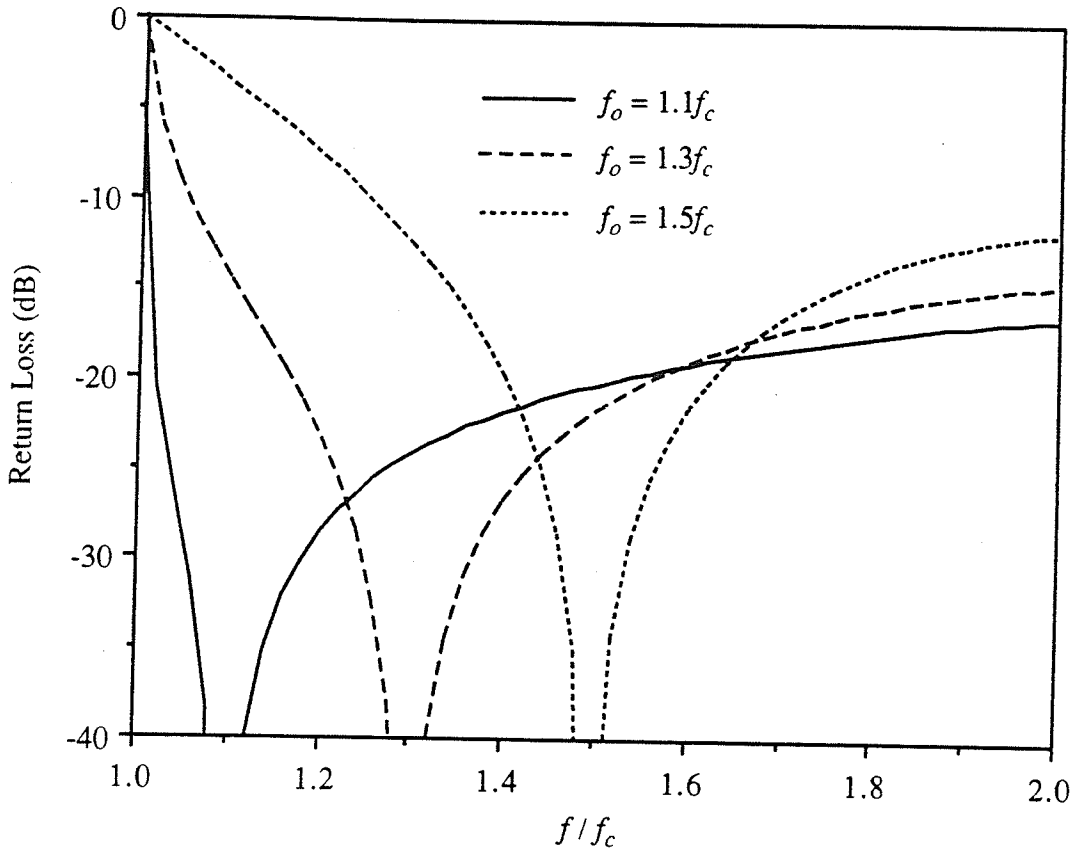

Fig. 3.16. Return loss as a function of normalized frequency for an iris matched dielectric window optimized for f_o / f_c = 1.1, 1.3, and 1.5 with ε_r = 2.8, L/a = 0.03, and $L_i = 5L$.

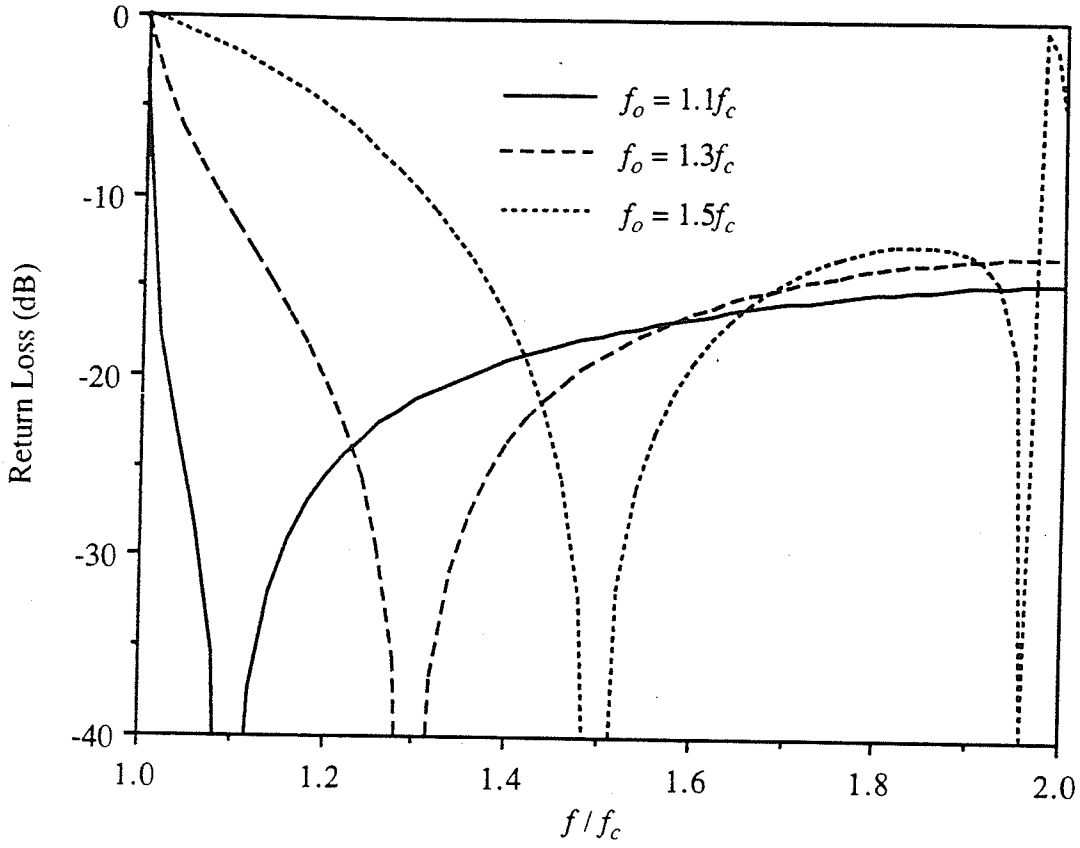

Fig. 3.17. Return loss as a function of normalized frequency for an iris matched dielectric window optimized for f_o / f_c = 1.1, 1.3, and 1.5 with ε_r = 2.8, L/a = 0.04, and $L_i = 5L$.

The choice of ten modes in each waveguide region was made in [18] partially on the basis of maintaining a reasonable computational time. Using a larger number of modes, as done here, would have dramatically increased the computation time for the optimization procedure. Table 3.11 shows the size and number of full complex matrix inversions required by the proposed method compared with cascading as in [18]. It is assumed that the dielectric region is bisected with an electric and magnetic wall to use the even and odd mode excitation analysis about the symmetry plane. The proposed formulation proves to be a more efficient method by requiring only two relatively small matrix inversions, compared to six matrix inversions in [18]. This allows more modes to used than in [18] without a large increase in computation time.

In Table 3.12, the minimum number of full complex matrix multiplications and inversions required to calculate the scattering parameters for N discontinuities is compared with the commonly used cascading techniques. The proposed formulation has a definite advantage over the two cascading techniques by requiring fewer matrix multiplications and inversions. Compared to the proposed formulation, cascading generalized scattering matrices (S-Matrix) [8] requires almost twice as many matrix multiplications and three times as many matrix inversions, and the transmission matrix method (T-Matrix) [5] requires almost 60 percent more matrix multiplications and two extra matrix inversions. The proposed formulation has the advantage over the transmission matrix method in being compatible with the criterion for avoiding the relative convergence phenomenon, which also gives the fastest convergence, and is numerically stable when the total length of the waveguide sections, $L_1 + L_2 + \ldots + L_N$, becomes large. A transmission matrix formulation compatible with the criterion for avoiding the relative convergence phenomenon has been presented in [8], but requires $2(N-1)$ additional matrix multiplications compared with [5].

Table 3.11

Comparison of number and size of full matrix inversions needed for matched dielectric window analysis.

	Number and Size of Inversions
Proposed Formulation	two N x N
Cascading [18]	two $(M+N)$ x $(M+N)$ two M x M two N x N

Table 3.12

Comparison of the minimum number of full matrix multiplications and inversions needed to calculate $\underline{\underline{S}}_{11}$ and $\underline{\underline{S}}_{21}$ for N discontinuities.

N	Proposed Formulation		S-matrix [8]		T-matrix [5]	
	Mult	Inv	Mult	Inv	Mult	Inv
2	7	1	13	3	11	3
3	12	2	28	6	19	4
4	17	3	43	9	27	5
5	22	4	58	12	35	6

CHAPTER 4

IMPROVED MODELLING WITH RESTRICTED HIGHER ORDER MODE INTERACTION

In order to extend the range of applicability of the general method in Chapter 2, for very large distances between discontinuities, a modified formulation is presented in this chapter. Consider the multiple-step discontinuities shown in Fig. 2.1. There are N transverse discontinuities with N+1 waveguide regions. An arbitrary multi-mode incident field is assumed from waveguide 1.

In the Chapter 2 formulation, all the modes retained in each region after truncation were assumed to be interacting with the adjacent discontinuities. The effect of the higher order modes can result in numerical instabilities as the separation distance between discontinuities increases. Reducing the number of modes alleviated the numerical difficulties by eliminating the destabilizing higher order modes in the truncation, but the accuracy of the solution may be compromised by the reduction in the number of modes.

The problem can be reformulated so that the modes allowed to interact are restricted, without compromising the accuracy, by classifying the modes in each region as interacting or non-interacting. The interacting modes will be defined as the modes that effectively interact between discontinuities, which includes all the propagating modes and the lower order evanescent modes up to a level which is to be determined. The non-interacting modes will be defined as the higher order evanescent modes that are excited at a discontinuity but do not effectively interact with the adjacent discontinuities. In this modified formulation, a finite number of non-interacting modes will be effectively matched terminated at the discontinuities, thereby eliminating their destabilizing effect. The total number of modes in each region can be chosen as large as needed to accurately describe the scattering at each discontinuity.

This modified formulation parallels the analysis in Chapter 2 with the exception that the modes in each region are partitioned into the interacting and the non-interacting cases.

4.1 Modal Expansions of the Fields

The total transverse electric and magnetic fields can be written in modal form as follows:

in the 1st region

$$\boldsymbol{E}_{t1} = \sum_m \left(A_{1m}\, e^{-\gamma_{1m}(z+z_1)} + B_{1m}\, e^{\gamma_{1m}(z+z_1)}\right)\boldsymbol{e}_{1m}$$

$$\boldsymbol{H}_{t1} = \sum_m \left(A_{1m}\, e^{-\gamma_{1m}(z+z_1)} - B_{1m}\, e^{\gamma_{1m}(z+z_1)}\right)\boldsymbol{h}_{1m}, \tag{4.1}$$

in the jth region ($j = 2, \ldots, N$)

$$\boldsymbol{E}_{tj} = \sum_m \left(A_{jm}\, e^{-\gamma_{jm}(z+z_{j-1})} + B_{jm}\, e^{\gamma_{jm}(z+z_j)}\right)\boldsymbol{e}_{jm}$$

$$\boldsymbol{H}_{tj} = \sum_m \left(A_{jm}\, e^{-\gamma_{jm}(z+z_{j-1})} - B_{jm}\, e^{\gamma_{jm}(z+z_j)}\right)\boldsymbol{h}_{jm}, \tag{4.2}$$

and in the N+1th region

$$\boldsymbol{E}_{t,N+1} = \sum_m A_{N+1,m}\, e^{-\gamma_{N+1,m}\, z}\, \boldsymbol{e}_{N+1,m}$$

$$\boldsymbol{H}_{t,N+1} = \sum_m A_{N+1,m}\, e^{-\gamma_{N+1,m}\, z}\, \boldsymbol{h}_{N+1,m}. \tag{4.3}$$

A_{im} and B_{im} are the forward and the backward complex coefficients, respectively, of the mth mode in the ith region, γ_{im} is the propagation constant, and $\boldsymbol{e}_{im}$ and $\boldsymbol{h}_{im}$ are the corresponding transverse electric and magnetic field functions of the mth mode. The modal field functions form an orthonormal set, *i.e.*,

$$\langle \boldsymbol{e}_{im}, \boldsymbol{h}_{in} \rangle_{S_i} = \int_{S_i} (\boldsymbol{e}_{im} \times \boldsymbol{h}_{in}) \cdot d\boldsymbol{s} = \delta_{mn} \tag{4.4}$$

where S_i is the ith waveguide cross section, and δ_{mn} is the Kronecker delta.

4.2 Boundary Conditions at the Discontinuity Planes

At each discontinuity plane, the transverse fields must be continuous over each aperture and the tangential electric field must be zero on the walls. The continuity of the transverse electric and magnetic field intensities over each aperture cross section are expressed as follows:

at $z = -z_1$

$$\sum_n (A_{1n} + B_{1n})\boldsymbol{e}_{1n} = \sum_n (A_{2n} + B_{2n}\, e^{-\gamma_{2n} L_2})\boldsymbol{e}_{2n} + \sum_p A_{2p}\, \boldsymbol{e}_{2p}$$

$$\sum_n (A_{1n} - B_{1n})\boldsymbol{h}_{1n} = \sum_n (A_{2n} - B_{2n}\, e^{-\gamma_{2n} L_2})\boldsymbol{h}_{2n} + \sum_p A_{2p}\, \boldsymbol{h}_{2p}, \qquad (4.5)$$

at $z = -z_j$ $(j = 2, \ldots, N)$

$$\sum_n (A_{jn}\, e^{-\gamma_{jn} L_j} + B_{jn})\boldsymbol{e}_{jn} + \sum_p B_{jp}\, \boldsymbol{e}_{jp} =$$

$$\sum_n (A_{j+1,n} + B_{j+1,n}\, e^{-\gamma_{j+1,n} L_{j+1}})\boldsymbol{e}_{j+1,n} + \sum_p A_{j+1,p}\, \boldsymbol{e}_{j+1,p}$$

$$\sum_n (A_{jn}\, e^{-\gamma_{jn} L_j} - B_{jn})\boldsymbol{h}_{jn} - \sum_p B_{jp}\, \boldsymbol{h}_{jp} =$$

$$\sum_n (A_{j+1,n} - B_{j+1,n}\, e^{-\gamma_{j+1,n} L_{j+1}})\boldsymbol{h}_{j+1,n} + \sum_p A_{j+1,p}\, \boldsymbol{h}_{j+1,p}, \qquad (4.6)$$

and at $z = 0$

$$\sum_n (A_{Nn}\, e^{-\gamma_{Nn} L_N} + B_{Nn})\boldsymbol{e}_{Nn} + \sum_p B_{Np}\, \boldsymbol{e}_{Np} = \sum_n A_{N+1,n}\, \boldsymbol{e}_{N+1,n}$$

$$\sum_n (A_{Nn}\, e^{-\gamma_{Nn} L_N} - B_{Nn})\boldsymbol{h}_{Nn} - \sum_p B_{Np}\, \boldsymbol{h}_{Np} = \sum_n A_{N+1,n}\, \boldsymbol{h}_{N+1,n} \qquad (4.7)$$

where

$$L_i \equiv -z_i + z_{i-1} \quad (i = 2, \ldots, N). \qquad (4.8)$$

The n and p subscripts refer to the interacting and the non-interacting modes, respectively. Since the non-interacting modes are not allowed to interact with the adjacent discontinuities, only the pth modes excited away from each discontinuity are included in the summations.

4.3 Matrix Equations for the Discontinuities

The orthogonality of the modes is applied to the field continuity equations, (4.5)-(4.7), to form linear equations that are truncated and expressed in matrix form. The boundary enlargement and reduction discontinuity cases are handled separately in order to properly include the boundary condition on the transverse walls [17], [18].

4.3.1 Boundary Enlargement Discontinuities

For the boundary enlargement case, at each discontinuity we take the vector product of the terms in the electric field continuity equation with a magnetic mode function from the following waveguide section, and the vector product of the terms in the magnetic field continuity equation with an electric mode function from the preceding waveguide section. Equations (4.5)-(4.7) become:

at $z = -z_1$

$$\sum_n (A_{1n} + B_{1n})\langle \boldsymbol{e}_{1n}, \boldsymbol{h}_{2m}\rangle_{S_1} = \sum_n (F_{2n}\cosh(\gamma_{2n}L_2) + D_{2n}\sinh(\gamma_{2n}L_2))\langle \boldsymbol{e}_{2n}, \boldsymbol{h}_{2m}\rangle_{S_2} + \sum_p A_{2p}\langle \boldsymbol{e}_{2p}, \boldsymbol{h}_{2m}\rangle_{S_2} \quad (m = 1, 2, 3...)$$

$$\sum_n (A_{1n} - B_{1n})\langle \boldsymbol{e}_{1m}, \boldsymbol{h}_{1n}\rangle_{S_1} = \sum_n (D_{2n}\cosh(\gamma_{2n}L_2) + F_{2n}\sinh(\gamma_{2n}L_2))\langle \boldsymbol{e}_{1m}, \boldsymbol{h}_{2n}\rangle_{S_1} + \sum_p A_{2p}\langle \boldsymbol{e}_{1m}, \boldsymbol{h}_{2p}\rangle_{S_1} \quad (m = 1, 2, 3...), \qquad (4.9)$$

at $z = -z_j$ $(j \neq 1, N)$

$$\sum_n F_{jn} \langle \boldsymbol{e}_{jn}, \boldsymbol{h}_{j+1,m} \rangle_{S_j} + \sum_p B_{jp} \langle \boldsymbol{e}_{jp}, \boldsymbol{h}_{j+1,m} \rangle_{S_j} =$$

$$\sum_n (F_{j+1,n} \cosh(\gamma_{j+1,n} L_{j+1}) + D_{j+1,n} \sinh(\gamma_{j+1,n} L_{j+1})) \langle \boldsymbol{e}_{j+1,n}, \boldsymbol{h}_{j+1,m} \rangle_{S_{j+1}}$$

$$+ \sum_p A_{j+1,p} \langle \boldsymbol{e}_{j+1,p}, \boldsymbol{h}_{j+1,m} \rangle_{S_{j+1}} \quad (m = 1, 2, 3...)$$

$$\sum_n D_{jn} \langle \boldsymbol{e}_{jm}, \boldsymbol{h}_{jn} \rangle_{S_j} - \sum_p B_{jp} \langle \boldsymbol{e}_{jm}, \boldsymbol{h}_{jp} \rangle_{S_j} =$$

$$\sum_n (D_{j+1,n} \cosh(\gamma_{j+1,n} L_{j+1}) + F_{j+1,n} \sinh(\gamma_{j+1,n} L_{j+1})) \langle \boldsymbol{e}_{jm}, \boldsymbol{h}_{j+1,n} \rangle_{S_j}$$

$$+ \sum_p A_{j+1,p} \langle \boldsymbol{e}_{jm}, \boldsymbol{h}_{j+1,p} \rangle_{S_j} \quad (n = 1, 2, 3...), \tag{4.10}$$

and at $z = 0$

$$\sum_n F_{Nn} \langle \boldsymbol{e}_{Nn}, \boldsymbol{h}_{N+1,m} \rangle_{S_N} + \sum_p B_{Np} \langle \boldsymbol{e}_{Np}, \boldsymbol{h}_{N+1,m} \rangle_{S_N} =$$

$$\sum_n A_{N+1,n} \langle \boldsymbol{e}_{N+1,n}, \boldsymbol{h}_{N+1,m} \rangle_{S_{N+1}} \quad (m = 1, 2, 3...)$$

$$\sum_n D_{Nn} \langle \boldsymbol{e}_{Nm}, \boldsymbol{h}_{Nn} \rangle_{S_N} - \sum_p B_{Np} \langle \boldsymbol{e}_{Nm}, \boldsymbol{h}_{Np} \rangle_{S_N} =$$

$$\sum_n A_{N+1,n} \langle \boldsymbol{e}_{Nm}, \boldsymbol{h}_{N+1,n} \rangle_{S_N} \quad (m = 1, 2, 3...) \tag{4.11}$$

where

$$D_{in} \equiv A_{in} e^{-\gamma_{in} L_i} - B_{in} \tag{4.12}$$

$$F_{in} \equiv A_{in} e^{-\gamma_{in} L_i} + B_{in} . \tag{4.13}$$

The infinite series are truncated to M_i modes in each ith region, where N_i of the modes are classified as interacting modes. Applying the mode orthogonality, equations (4.9)-(4.11) can be written in matrix form:

at $z = -z_1$

$$\underline{\underline{G}}_1 (\underline{A}_1 + \underline{B}_1) = \underline{\underline{C}}_2 \underline{F}_2 + \underline{\underline{S}}_2 \underline{D}_2$$

$$\underline{\underline{H}}_1 (\underline{A}_1 + \underline{B}_1) = \underline{A}_2$$

$$\underline{A}_1 - \underline{B}_1 = \underline{\underline{G}}_1^T (\underline{\underline{C}}_2 \underline{D}_2 + \underline{\underline{S}}_2 \underline{F}_2) + \underline{\underline{H}}_1^T \underline{A}_2, \tag{4.14}$$

at $z = -z_j \ (j \neq 1, N)$

$$\underline{\underline{G}}_j \underline{F}_j + \underline{\underline{P}}_j \underline{B}_j = \underline{\underline{C}}_{j+1} \underline{F}_{j+1} + \underline{\underline{S}}_{j+1} \underline{D}_{j+1}$$

$$\underline{\underline{H}}_j \underline{F}_j + \underline{\underline{K}}_j \underline{B}_j = \underline{A}_{j+1}$$

$$\underline{D}_j = \underline{\underline{G}}_j^T (\underline{\underline{C}}_{j+1} \underline{D}_{j+1} + \underline{\underline{S}}_{j+1} \underline{F}_{j+1}) + \underline{\underline{H}}_j^T \underline{A}_{j+1}$$

$$-\underline{B}_j = \underline{\underline{P}}_j^T (\underline{\underline{C}}_{j+1} \underline{D}_{j+1} + \underline{\underline{S}}_{j+1} \underline{F}_{j+1}) + \underline{\underline{K}}_j^T \underline{A}_{j+1}, \tag{4.15}$$

and at $z = 0$

$$\underline{\underline{G}}_N \underline{F}_N + \underline{\underline{P}}_N \underline{B}_N = \underline{A}_{N+1}$$

$$\underline{D}_N = \underline{\underline{G}}_N^T \underline{A}_{N+1}$$

$$-\underline{B}_N = \underline{\underline{P}}_N^T \underline{A}_{N+1} \tag{4.16}$$

where the T superscript indicates matrix transpose, $\underline{A}_1$ is the known incident modal coefficient column matrix of M_1 elements, $\underline{B}_1$ and $\underline{A}_{N+1}$ are the column matrices of M_1 and M_{N+1} elements of the unknown modal coefficients for the fields reflected in region 1 and transmitted in region N+1, respectively, $\underline{A}_i$ and $\underline{B}_i$ are the forward and the backward

non-interacting modal coefficient column matrices in region i ($i \neq 1, N$), respectively, of $M_i - N_i$ elements, and

$$\underline{D}_i = \left[A_{im}\, e^{-\gamma_{im} L_i} - B_{im} \right]_{M_i \text{ x } 1} \tag{4.17}$$

$$\underline{F}_i = \left[A_{im}\, e^{-\gamma_{im} L_i} + B_{im} \right]_{M_i \text{ x } 1} \tag{4.18}$$

$$\underline{\underline{C}}_i = \left[\delta_{mn} \cosh(\gamma_{im} L_i) \right]_{M_i \text{ x } M_i} \tag{4.19}$$

$$\underline{\underline{S}}_i = \left[\delta_{mn} \sinh(\gamma_{im} L_i) \right]_{M_i \text{ x } M_i} \tag{4.20}$$

$$\underline{\underline{G}}_i = \left[\langle \boldsymbol{e}_{in}, \boldsymbol{h}_{i+1,m} \rangle_{S_i} \right]_{N_{i+1} \text{ x } M_i} \tag{4.21}$$

$$\underline{\underline{P}}_i = \left[\langle \boldsymbol{e}_{ip}, \boldsymbol{h}_{i+1,m} \rangle_{S_i} \right]_{N_{i+1} \text{ x } (M_i - N_i)} \tag{4.22}$$

$$\underline{\underline{H}}_i = \left[\langle \boldsymbol{e}_{in}, \boldsymbol{h}_{i+1,m} \rangle_{S_i} \right]_{(M_{i+1} - N_{i+1}) \text{ x } M_i} \tag{4.23}$$

$$\underline{\underline{K}}_i = \left[\langle \boldsymbol{e}_{ip}, \boldsymbol{h}_{i+1,m} \rangle_{S_i} \right]_{(M_{i+1} - N_{i+1}) \text{ x } (M_i - N_i)}. \tag{4.24}$$

4.3.2 Boundary Reduction Discontinuities

For the boundary reduction case, at each discontinuity we take the vector product of the terms in the electric field continuity equation with a magnetic mode function from the preceding waveguide section, and the vector product of the terms in the magnetic field continuity equation with an electric mode function from the following waveguide section. Equations (4.5)-(4.7) become:

at $z = -z_1$

$$\sum_n (A_{1n} + B_{1n}) \langle \boldsymbol{e}_{1n}, \boldsymbol{h}_{1m} \rangle_{S_1} = \sum_n (F_{2n} \cosh(\gamma_{2n} L_2) + D_{2n} \sinh(\gamma_{2n} L_2)) \langle \boldsymbol{e}_{2n}, \boldsymbol{h}_{1m} \rangle_{S_2}$$

$$+ \sum_p A_{2p} \langle \boldsymbol{e}_{2p}, \boldsymbol{h}_{1m} \rangle_{S_2} \quad (m = 1, 2, 3...)$$

$$\sum_n (A_{1n} - B_{1n})\langle \boldsymbol{e}_{2m}, \boldsymbol{h}_{1n}\rangle_{S_2} = \sum_n (D_{2n}\cosh(\gamma_{2n}L_2) + F_{2n}\sinh(\gamma_{2n}L_2))\langle \boldsymbol{e}_{2m}, \boldsymbol{h}_{2n}\rangle_{S_2}$$

$$+ \sum_p A_{2p}\langle \boldsymbol{e}_{2m}, \boldsymbol{h}_{2p}\rangle_{S_2} \quad (m = 1, 2, 3...), \tag{4.25}$$

at $z = -z_j$ $(j \neq 1, N)$

$$\sum_n F_{jn}\langle \boldsymbol{e}_{jn}, \boldsymbol{h}_{jm}\rangle_{S_j} + \sum_p B_{jp}\langle \boldsymbol{e}_{jp}, \boldsymbol{h}_{jm}\rangle_{S_j} =$$

$$\sum_n (F_{j+1,n}\cosh(\gamma_{j+1,n}L_{j+1}) + D_{j+1,n}\sinh(\gamma_{j+1,n}L_{j+1}))\langle \boldsymbol{e}_{j+1,n}, \boldsymbol{h}_{jm}\rangle_{S_{j+1}}$$

$$+ \sum_p A_{j+1,p}\langle \boldsymbol{e}_{j+1,p}, \boldsymbol{h}_{jm}\rangle_{S_{j+1}} \quad (m = 1, 2, 3...)$$

$$\sum_n D_{jn}\langle \boldsymbol{e}_{j+1,m}, \boldsymbol{h}_{jn}\rangle_{S_{j+1}} - \sum_p B_{jp}\langle \boldsymbol{e}_{j+1,m}, \boldsymbol{h}_{jp}\rangle_{S_{j+1}} =$$

$$\sum_n (D_{j+1,n}\cosh(\gamma_{j+1,n}L_{j+1}) + F_{j+1,n}\sinh(\gamma_{j+1,n}L_{j+1}))\langle \boldsymbol{e}_{j+1,m}, \boldsymbol{h}_{j+1,n}\rangle_{S_{j+1}}$$

$$+ \sum_p A_{j+1,p}\langle \boldsymbol{e}_{j+1,m}, \boldsymbol{h}_{j+1,p}\rangle_{S_{j+1}} \quad (m = 1, 2, 3...), \tag{4.26}$$

and at $z = 0$

$$\sum_n F_{Nn}\langle \boldsymbol{e}_{Nn}, \boldsymbol{h}_{Nm}\rangle_{S_N} + \sum_p B_{Np}\langle \boldsymbol{e}_{Np}, \boldsymbol{h}_{Nm}\rangle_{S_N} =$$

$$\sum_n A_{N+1,n}\langle \boldsymbol{e}_{N+1,n}, \boldsymbol{h}_{Nm}\rangle_{S_{N+1}} \quad (m = 1, 2, 3...)$$

$$\sum_n D_{Nn}\langle \boldsymbol{e}_{N+1,m}, \boldsymbol{h}_{Nn}\rangle_{S_{N+1}} - \sum_p B_{Np}\langle \boldsymbol{e}_{N+1,m}, \boldsymbol{h}_{Np}\rangle_{S_{N+1}} =$$

$$\sum_n A_{N+1,n}\langle \boldsymbol{e}_{N+1,m}, \boldsymbol{h}_{N+1,n}\rangle_{S_{N+1}} \quad (m = 1, 2, 3...) \tag{4.27}$$

where D_{in} and F_{in} are defined in (4.12) and (4.13), respectively.

As before, the infinite series are truncated to M_i modes in each ith region, where N_i of the modes are classified as interacting modes. Applying the mode orthogonality, equations (4.25)-(4.27) can be written in matrix form:

at $z = -z_1$

$$\underline{A}_1 + \underline{B}_1 = \underline{\underline{G}}_1^T (\underline{\underline{C}}_2 \underline{F}_2 + \underline{\underline{S}}_2 \underline{D}_2) + \underline{\underline{H}}_1^T \underline{A}_2$$

$$\underline{\underline{G}}_1 (\underline{A}_1 - \underline{B}_1) = \underline{\underline{C}}_2 \underline{D}_2 + \underline{\underline{S}}_2 \underline{F}_2$$

$$\underline{\underline{H}}_1 (\underline{A}_1 - \underline{B}_1) = \underline{A}_2, \tag{4.28}$$

at $z = -z_j$ $(j \neq 1, N)$

$$\underline{F}_j = \underline{\underline{G}}_j^T (\underline{\underline{C}}_{j+1} \underline{F}_{j+1} + \underline{\underline{S}}_{j+1} \underline{D}_{j+1}) + \underline{\underline{H}}_j^T \underline{A}_{j+1}$$

$$\underline{B}_j = \underline{\underline{P}}_j^T (\underline{\underline{C}}_{j+1} \underline{F}_{j+1} + \underline{\underline{S}}_{j+1} \underline{D}_{j+1}) + \underline{\underline{K}}_j^T \underline{A}_{j+1}$$

$$\underline{\underline{G}}_j \underline{D}_j - \underline{\underline{P}}_j \underline{B}_j = \underline{\underline{C}}_{j+1} \underline{D}_{j+1} + \underline{\underline{S}}_{j+1} \underline{F}_{j+1}$$

$$\underline{\underline{H}}_j \underline{D}_j - \underline{\underline{K}}_j \underline{B}_j = \underline{A}_{j+1}, \tag{4.29}$$

and at $z = 0$

$$\underline{F}_N = \underline{\underline{G}}_N^T \underline{A}_{N+1}$$

$$\underline{B}_N = \underline{\underline{P}}_N^T \underline{A}_{N+1}$$

$$\underline{\underline{G}}_N \underline{D}_N - \underline{\underline{P}}_N \underline{B}_N = \underline{A}_{N+1} \tag{4.30}$$

where the quantities are described in (4.17)-(4.20), except in the boundary reduction case

$$\underline{\underline{G}}_i = \left[\langle \boldsymbol{e}_{i+1,m}, \boldsymbol{h}_{in} \rangle_{S_{i+1}} \right]_{N_{i+1} \text{ x } M_i} \tag{4.31}$$

$$\underline{\underline{P}}_i = \left[\langle \boldsymbol{e}_{i+1,m}, \boldsymbol{h}_{ip} \rangle_{S_{i+1}} \right]_{N_{i+1} \text{ x } (M_i - N_i)} \tag{4.32}$$

$$\underline{\underline{H}}_i = \left[\langle \boldsymbol{e}_{i+1,m}, \boldsymbol{h}_{in} \rangle_{S_{i+1}} \right]_{(M_{i+1} - N_{i+1}) \text{ x } M_i} \tag{4.33}$$

$$\underline{\underline{K}}_i = \left[\langle \boldsymbol{e}_{i+1,m}, \boldsymbol{h}_{ip} \rangle_{S_{i+1}} \right]_{(M_{i+1} - N_{i+1}) \text{ x } (M_i - N_{i+1})}. \tag{4.34}$$

The sets of linear matrix equations for an arbitrary combination of boundary enlargement and reduction discontinuities can be compiled by considering the corresponding matrix equations in (4.14)-(4.16) or (4.27)-(4.30).

4.4 Scattering Matrix Formulation

In scattering matrix formulation, $\underline{B}_1$ and $\underline{A}_{N+1}$ can be expressed as

$$\underline{B}_1 = \underline{\underline{S}}_{11} \underline{A}_1$$

$$\underline{A}_{N+1} = \underline{\underline{S}}_{21} \underline{A}_1 \tag{4.35}$$

where $\underline{\underline{S}}_{11}$ and $\underline{\underline{S}}_{21}$ are the complex reflection and transmission matrices for the entire structure, respectively. Solving the sets of linear matrix equations for an arbitrary series of boundary enlargement and reduction discontinuities, the scattering matrices are obtained as

$$\underline{\underline{S}}_{11} = \begin{cases} \left(\underline{\underline{I}} + \underline{\underline{H}}_1^T \underline{\underline{H}}_1\right)^{-1} \left[\left(\underline{\underline{I}} - \underline{\underline{H}}_1^T \underline{\underline{H}}_1\right) - 2\, \underline{\underline{G}}_1^T \underline{\underline{Q}}_2 \underline{\underline{U}}^{-1} \underline{\underline{G}}_1 \left(\underline{\underline{I}} + \underline{\underline{H}}_1^T \underline{\underline{H}}_1\right)^{-1}\right], \text{ for a 1st} \\ \qquad\qquad \text{discontinuity boundary enlargement (B.E.)} \\ \left(\underline{\underline{I}} + \underline{\underline{H}}_1^T \underline{\underline{H}}_I\right)^{-1} \left[-\left(\underline{\underline{I}} - \underline{\underline{H}}_1^T \underline{\underline{H}}_1\right) + 2\, \underline{\underline{G}}_1^T \underline{\underline{Q}}_2 \underline{\underline{U}}^{-1} \underline{\underline{G}}_1 \left(\underline{\underline{I}} + \underline{\underline{H}}_1^T \underline{\underline{H}}_1\right)^{-1}\right], \text{ for a 1st} \\ \qquad\qquad \text{discontinuity boundary reduction (B.R.)} \end{cases} \tag{4.36}$$

$$\underline{\underline{S}}_{21} = 2 \left(\underline{\underline{I}} + \underline{\underline{P}}_N^T \underline{\underline{P}}_N\right)^{-1} \left(\underline{\underline{G}}_N \underline{\underline{R}}_N^{-1}\right) \left(\hat{\underline{\underline{G}}}_{N-1} \underline{\underline{R}}_{N-1}^{-1}\right) \ldots \left(\hat{\underline{\underline{G}}}_3 \underline{\underline{R}}_3^{-1}\right) \hat{\underline{\underline{G}}}_2 \underline{\underline{U}}^{-1} \underline{\underline{G}}_1 \left(\underline{\underline{I}} + \underline{\underline{H}}_1^T \underline{\underline{H}}_1\right)^{-1} \tag{4.37}$$

where $\underline{\underline{G}}_i$, $\underline{\underline{P}}_i$, $\underline{\underline{H}}_i$, and $\underline{\underline{K}}_i$ are described in equations (4.21)-(4.24) or (4.31)-(4.34) for the

ith discontinuity B.E or B.R. case, respectively, $\underline{\underline{I}}$ is the unit matrix,

$$\underline{\underline{U}} = \begin{cases} (\underline{\underline{C}}_2 + \underline{\underline{G}}_1 (\underline{\underline{I}} + \underline{\underline{H}}_1^T \underline{\underline{H}}_1)^{-1} \underline{\underline{G}}_1^T \underline{\underline{S}}_2) \\ + (\underline{\underline{S}}_2 + \underline{\underline{G}}_1 (\underline{\underline{I}} + \underline{\underline{H}}_1^T \underline{\underline{H}}_1)^{-1} \underline{\underline{G}}_1^T \underline{\underline{C}}_2)(\underline{\underline{H}}_2^T (\underline{\underline{I}} + \underline{\underline{K}}_2^T \underline{\underline{K}}_2)^{-1} \underline{\underline{H}}_2 + \hat{\underline{\underline{G}}}_2^T \underline{\underline{Q}}_3 \underline{\underline{R}}_3^{-1} \hat{\underline{\underline{G}}}_2), \\ \qquad \text{for the 1st and 2nd discontinuities both B.E. or B.R.} \\ (\underline{\underline{S}}_2 + \underline{\underline{G}}_1 (\underline{\underline{I}} + \underline{\underline{H}}_1^T \underline{\underline{H}}_1)^{-1} \underline{\underline{G}}_1^T \underline{\underline{C}}_2) \\ + (\underline{\underline{C}}_2 + \underline{\underline{G}}_1 (\underline{\underline{I}} + \underline{\underline{H}}_1^T \underline{\underline{H}}_1)^{-1} \underline{\underline{G}}_1^T \underline{\underline{S}}_2)(\underline{\underline{H}}_2^T (\underline{\underline{I}} + \underline{\underline{K}}_2^T \underline{\underline{K}}_2)^{-1} \underline{\underline{H}}_2 + \hat{\underline{\underline{G}}}_2^T \underline{\underline{Q}}_3 \underline{\underline{R}}_3^{-1} \hat{\underline{\underline{G}}}_2), \\ \qquad \text{otherwise.} \end{cases} \tag{4.38}$$

$\underline{\underline{Q}}_i$ and $\underline{\underline{R}}_i$ are M_i x M_i matrices calculated from the following recurrence formulas:

$$\underline{\underline{Q}}_i = \begin{cases} \underline{\underline{S}}_i + \underline{\underline{C}}_i (\underline{\underline{H}}_i^T (\underline{\underline{I}} + \underline{\underline{K}}_i^T \underline{\underline{K}}_i)^{-1} \underline{\underline{H}}_i + \hat{\underline{\underline{G}}}_i^T \underline{\underline{Q}}_{i+1} \underline{\underline{R}}_{i+1}^{-1} \hat{\underline{\underline{G}}}_i), \text{ for the } i\text{th and } i\text{+1th} \\ \qquad \text{discontinuities both B.E. or B.R.} \\ \underline{\underline{C}}_i + \underline{\underline{S}}_i (\underline{\underline{H}}_i^T (\underline{\underline{I}} + \underline{\underline{K}}_i^T \underline{\underline{K}}_i)^{-1} \underline{\underline{H}}_i + \hat{\underline{\underline{G}}}_i^T \underline{\underline{Q}}_{i+1} \underline{\underline{R}}_{i+1}^{-1} \hat{\underline{\underline{G}}}_i), \text{ otherwise} \end{cases} \tag{4.39}$$

$$\underline{\underline{R}}_i = \begin{cases} \hat{\underline{\underline{C}}}_i + \hat{\underline{\underline{S}}}_i (\underline{\underline{H}}_i^T (\underline{\underline{I}} + \underline{\underline{K}}_i^T \underline{\underline{K}}_i)^{-1} \underline{\underline{H}}_i + \hat{\underline{\underline{G}}}_i^T \underline{\underline{Q}}_{i+1} \underline{\underline{R}}_{i+1}^{-1} \hat{\underline{\underline{G}}}_i), \text{ for the } i\text{th and } i\text{+1th} \\ \qquad \text{discontinuities both B.E. or B.R.} \\ \hat{\underline{\underline{S}}}_i + \hat{\underline{\underline{C}}}_i (\underline{\underline{H}}_i^T (\underline{\underline{I}} + \underline{\underline{K}}_i^T \underline{\underline{K}}_i)^{-1} \underline{\underline{H}}_i + \hat{\underline{\underline{G}}}_i^T \underline{\underline{Q}}_{i+1} \underline{\underline{R}}_{i+1}^{-1} \hat{\underline{\underline{G}}}_i)], \text{ otherwise} \end{cases} \tag{4.40}$$

with

$$\hat{\underline{\underline{G}}}_i = \underline{\underline{G}}_i + \underline{\underline{P}}_i (\underline{\underline{I}} + \underline{\underline{K}}_i^T \underline{\underline{K}}_i)^{-1} \underline{\underline{K}}_i^T \underline{\underline{H}}_i \tag{4.41}$$

$$\hat{\underline{\underline{S}}}_i = \underline{\underline{S}}_i + \underline{\underline{P}}_{i-1} (\underline{\underline{I}} + \underline{\underline{K}}_{i-1}^T \underline{\underline{K}}_{i-1})^{-1} \underline{\underline{P}}_{i-1}^T \underline{\underline{C}}_i \tag{4.42}$$

$$\hat{\underline{\underline{C}}}_i = \underline{\underline{C}}_i + \underline{\underline{P}}_{i-1} (\underline{\underline{I}} + \underline{\underline{K}}_{i-1}^T \underline{\underline{K}}_{i-1})^{-1} \underline{\underline{P}}_{i-1}^T \underline{\underline{S}}_i \tag{4.43}$$

$$\underline{\underline{Q}}_N = \begin{cases} \underline{\underline{S}}_N + \underline{\underline{C}}_N \; \underline{\underline{G}}_N^T \left(\underline{\underline{I}} + \underline{\underline{P}}_N \underline{\underline{P}}_N^T \right)^{-1} \underline{\underline{G}}_N, \text{ for the } N\text{–1th and } N\text{th discontinuities} \\ \qquad\qquad\qquad\qquad\qquad\qquad\qquad\qquad\qquad\qquad\qquad\qquad \text{both B.E. or B.R.} \\ \underline{\underline{C}}_N + \underline{\underline{S}}_N \; \underline{\underline{G}}_N^T \left(\underline{\underline{I}} + \underline{\underline{P}}_N \underline{\underline{P}}_N^T \right)^{-1} \underline{\underline{G}}_N, \text{ otherwise} \end{cases} \tag{4.44}$$

$$\underline{\underline{R}}_N = \begin{cases} \hat{\underline{\underline{C}}}_N + \hat{\underline{\underline{S}}}_N \; \underline{\underline{G}}_N^T \left(\underline{\underline{I}} + \underline{\underline{P}}_N \underline{\underline{P}}_N^T \right)^{-1} \underline{\underline{G}}_N, \text{ for the } N\text{–1th and } N\text{th discontinuities} \\ \qquad\qquad\qquad\qquad\qquad\qquad\qquad\qquad\qquad\qquad\qquad\qquad \text{both B.E. or B.R.} \\ \hat{\underline{\underline{S}}}_N + \hat{\underline{\underline{C}}}_N \; \underline{\underline{G}}_N^T \left(\underline{\underline{I}} + \underline{\underline{P}}_N \underline{\underline{P}}_N^T \right)^{-1} \underline{\underline{G}}_N, \text{ otherwise.} \end{cases} \tag{4.45}$$

In equations (4.36)-(4.45), the following identities can be used for $\underline{\underline{Z}} \equiv \underline{\underline{P}}_i$, $\underline{\underline{H}}_i$, or $\underline{\underline{K}}_i$:

$$2 \left(\underline{\underline{I}} + \underline{\underline{Z}}^T \underline{\underline{Z}} \right)^{-1} \equiv \underline{\underline{I}} + \left(\underline{\underline{I}} + \underline{\underline{Z}}^T \underline{\underline{Z}} \right)^{-1} \left(\underline{\underline{I}} - \underline{\underline{Z}}^T \underline{\underline{Z}} \right) \tag{4.46}$$

$$\left(\underline{\underline{I}} + \underline{\underline{Z}}^T \underline{\underline{Z}} \right)^{-1} \equiv \underline{\underline{I}} - \underline{\underline{Z}}^T \left(\underline{\underline{I}} + \underline{\underline{Z}} \; \underline{\underline{Z}}^T \right)^{-1} \underline{\underline{Z}} \tag{4.47}$$

$$\left(\underline{\underline{I}} + \underline{\underline{Z}} \; \underline{\underline{Z}}^T \right)^{-1} \equiv \underline{\underline{I}} - \underline{\underline{Z}} \left(\underline{\underline{I}} + \underline{\underline{Z}}^T \underline{\underline{Z}} \right)^{-1} \underline{\underline{Z}}^T \tag{4.48}$$

Proofs for the identities are shown in the Appendix.

4.5 Numerical Results for Circular Waveguides

A thick iris in a circular waveguide is studied quantitatively to determine a criterion for choosing the number of interacting modes in circular waveguides. Numerical results for a thick iris in a circular waveguide are compared with data available in the literature to verify the accuracy of the formulation. The technique is also applied to the analysis of step transformers in circular waveguides.

4.5.1 Convergence and Accuracy

Consider a thick circular iris of radius b and length L in a circular waveguide of radius a, as shown in Fig. 3.1. In the previous chapter, it was found that the optimum ratio of the number of modes for good convergence is $M/N \approx a/b$ where M and N are the total number of modes in waveguide regions and iris region, respectively. However, the number of interacting modes in the iris region P must be chosen sufficiently large enough to account for the higher order mode interaction between the discontinuities. A criterion for choosing the number of interacting modes can be established by studying the numerical results for an incident TE_{11} mode.

In Fig. 4.1 and Fig 4.2, the magnitude of the reflection coefficient is shown as a function of P, with $M = N(a/b) = 40$, for several values of L/a and ka. It is observed that the reflection coefficient typically converges when the evanescent modes with $\gamma L < 4$ are allowed to interact between the discontinuities in the iris region. All the propagating modes must be included in the truncations. Although good results may be obtained using fewer modes, this criterion serves as a general guideline for choosing the number of interacting modes in circular waveguides. Instability may occur if too many higher order modes are allowed to interact as can be seen for $L/a = 0.4$ in the figures. Comparison with numerical results calculated by the moment method [14] are shown in Table 4.1 through Table 4.8. The results are in excellent agreement for all values of L using $M = N(a/b) = 40$ and P as shown in the tables.

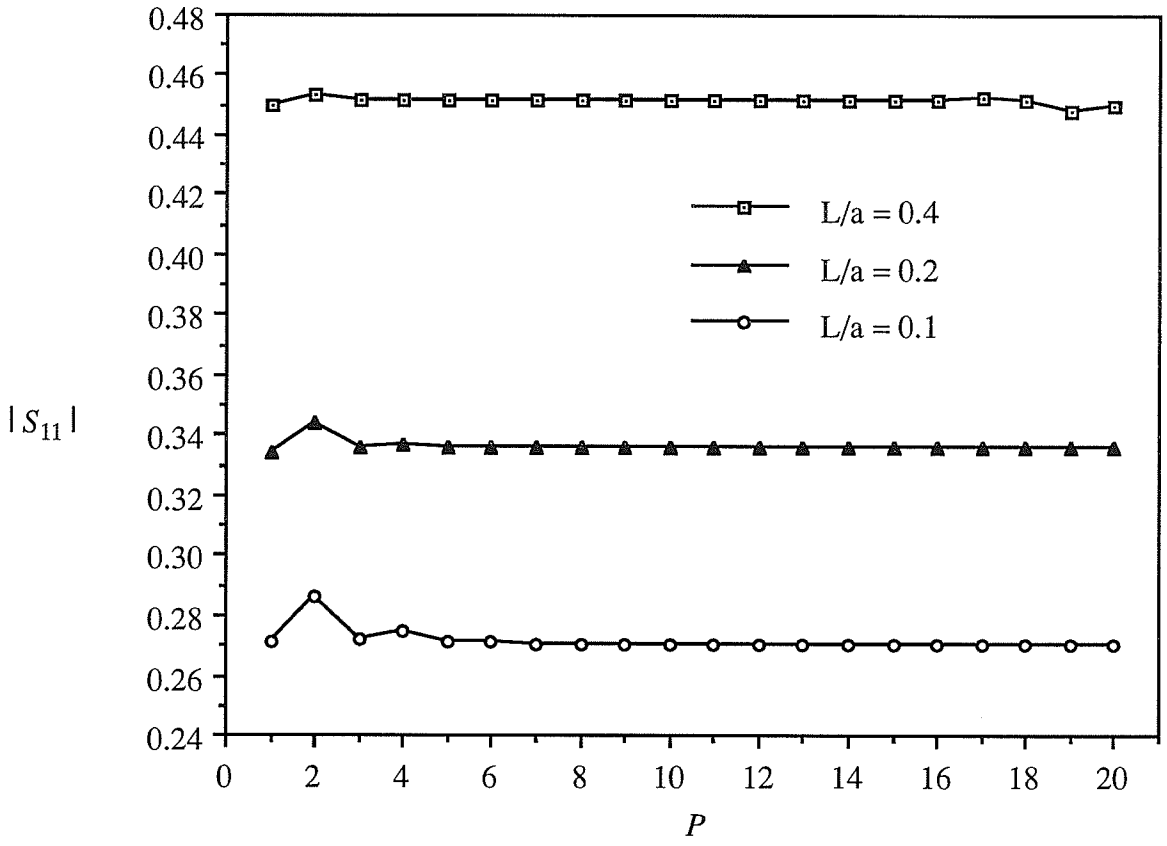

Fig. 4.1. Magnitude of the reflection coefficient as a function of P for a thick iris with $a = 1.338b$ and $ka = 2.4$.

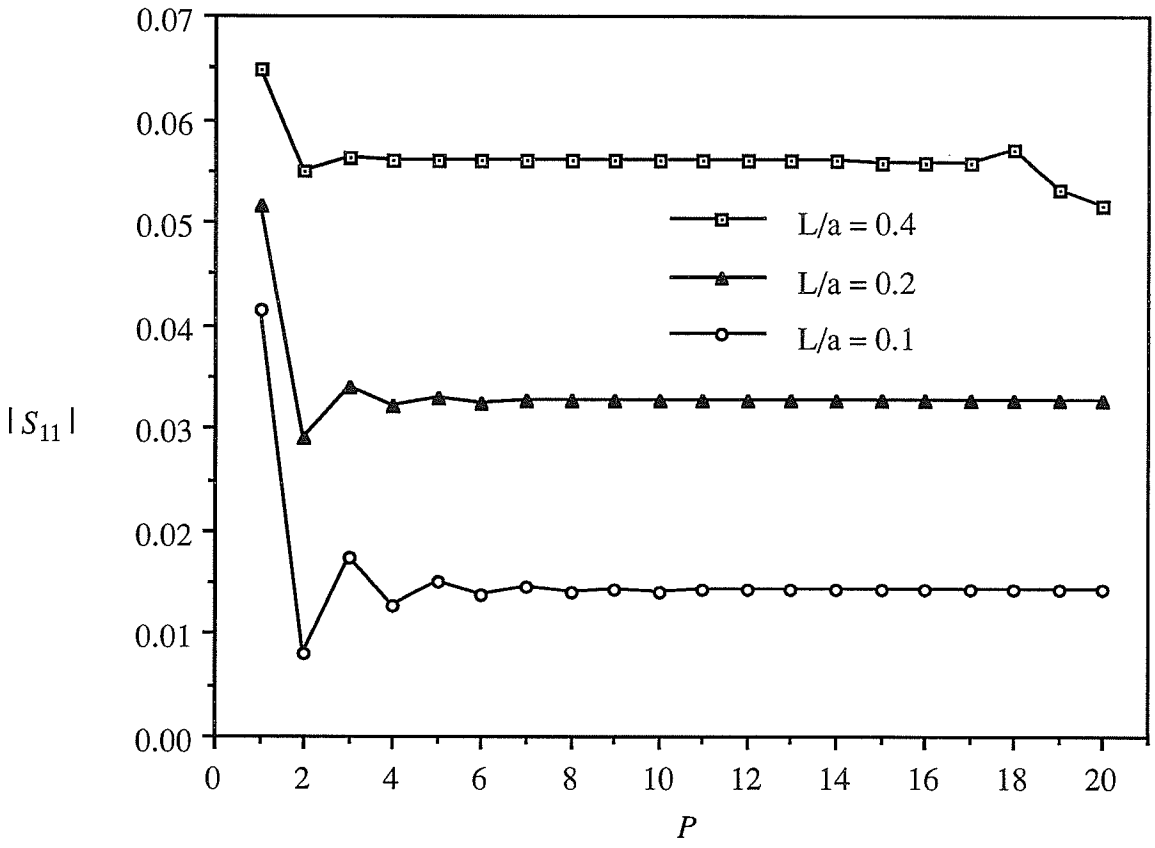

Fig. 4.2. Magnitude of the reflection coefficient as a function of P for a thick iris with $a = 1.338b$ and $ka = 3.2$.

Table 4.1

Comparison of the reflection coefficient as a function of L for a thick iris with $a = 0.50175$ in, $b = 0.25$ in, and $f = 9$ GHz.

L (inch)	Moment Method [14]		Proposed Formulation		
	Magnitude	Phase (degrees)	Magnitude	Phase (degrees)	P
0.050	0.934	155.7	0.934	155.6	12
0.100	0.966	158.6	0.965	158.6	6
0.200	0.990	161.0	0.989	160.9	3
0.500	1.000	162.0	1.000	162.0	1
1.000	1.000	162.0	1.000	162.0	1
3.000	1.000	162.0	1.000	162.0	1

Table 4.2

Comparison of the transmission coefficient as a function of L for a thick iris with $a = 0.50175$ in, $b = 0.25$ in, and $f = 9$ GHz.

L (inch)	Moment Method [14]		Proposed Formulation		
	Magnitude	Phase (degrees)	Magnitude	Phase (degrees)	P
0.050	0.356	65.7	0.358	65.6	12
0.100	0.260	68.6	0.261	68.6	6
0.200	0.144	71.0	0.145	70.9	3
0.500	0.027	72.0	0.027	72.0	1
1.000	0.002	72.0	0.002	72.0	1
3.000	0.000	75.7	0.000	72.0	1

Table 4.3

Comparison of the reflection coefficient as a function of L for a thick iris with $a = 0.50175$ in, $b = 0.25$ in, and $f = 12$ GHz.

L (inch)	Moment Method [14]		Proposed Formulation		
	Magnitude	Phase (degrees)	Magnitude	Phase (degrees)	P
0.050	0.488	113.2	0.486	113.0	12
0.100	0.622	116.8	0.620	116.6	6
0.200	0.806	122.0	0.804	121.9	3
0.500	0.977	127.4	0.977	127.3	1
1.000	0.999	128.1	0.999	128.0	1
3.000	1.000	128.2	1.000	128.0	1

Table 4.4

Comparison of the transmission coefficient as a function of L for a thick iris with $a = 0.50175$ in, $b = 0.25$ in, and $f = 12$ GHz.

L (inch)	Moment Method [14]		Proposed Formulation		
	Magnitude	Phase (degrees)	Magnitude	Phase (degrees)	P
0.050	0.873	23.2	0.874	23.0	12
0.100	0.783	26.8	0.784	26.6	6
0.200	0.593	32.0	0.594	31.9	3
0.500	0.211	37.4	0.212	37.3	1
1.000	0.034	38.1	0.034	38.0	1
3.000	0.000	38.1	0.000	38.0	1

Table 4.5

Comparison of the reflection coefficient as a function of L for a thick iris with $a = 0.50175$ in, $b = 0.375$ in, and $f = 9$ GHz.

L (inch)	Moment Method [14]		Proposed Formulation		
	Magnitude	Phase (degrees)	Magnitude	Phase (degrees)	P
0.050	0.272	99.3	0.270	99.2	15
0.100	0.337	97.0	0.336	96.9	10
0.200	0.453	92.4	0.452	92.3	5
0.500	0.706	82.0	0.705	81.9	2
1.000	0.901	73.4	0.900	73.2	1
3.000	0.999	68.7	0.999	68.5	1

Table 4.6

Comparison of the transmission coefficient as a function of L for a thick iris with $a = 0.50175$ in, $b = 0.375$ in, and $f = 9$ GHz.

L (inch)	Moment Method [14]		Proposed Formulation		
	Magnitude	Phase (degrees)	Magnitude	Phase (degrees)	P
0.050	0.962	9.3	0.963	9.2	15
0.100	0.941	7.0	0.942	6.9	10
0.200	0.892	2.4	0.892	2.3	5
0.500	0.708	–8.0	0.709	–8.1	2
1.000	0.434	–16.6	0.435	–16.8	1
3.000	0.052	–21.3	0.052	–21.5	1

Table 4.7

Comparison of the reflection coefficient as a function of L for a thick iris with $a = 0.50175$ in, $b = 0.375$ in, and $f = 12$ GHz.

L (inch)	Moment Method [14]		Proposed Formulation		
	Magnitude	Phase (degrees)	Magnitude	Phase (degrees)	P
0.050	0.014	–102.2	0.014	–102.1	15
0.100	0.033	–114.4	0.033	–114.4	10
0.200	0.056	–138.6	0.056	–138.6	5
0.500	0.040	150.8	0.040	150.8	2
1.000	0.067	–146.3	0.067	–146.3	1
3.000	0.010	–74.6	0.010	–74.7	1

Table 4.8

Comparison of the transmission coefficient as a function of L for a thick iris with $a = 0.50175$ in, $b = 0.375$ in, and $f = 12$ GHz.

L (inch)	Moment Method [14]		Proposed Formulation		
	Magnitude	Phase (degrees)	Magnitude	Phase (degrees)	P
0.050	1.000	–12.1	1.000	–12.1	15
0.100	0.999	–24.4	0.999	–24.4	10
0.200	0.998	–48.6	0.998	–48.6	5
0.500	0.999	–119.2	0.999	–119.2	2
1.000	0.998	123.7	0.998	123.7	1
3.000	1.000	15.4	1.000	15.4	1

4.5.2 Application to Step Transformers

Figure 4.3 shows step transformers that are used as transitions between waveguides of different dimensions. The dimensions for two- and four-section quarter-wave transformers in circular waveguides, designed by Sabatier *et. al.* [26], are given in Table 4.9. Comparison with numerical results for the voltage standing wave ratio (VSWR) of the two- and four-section transformers, calculated using the modal analysis technique with cascading [26], are shown in Fig. 4.4 and Fig. 4.5, respectively. Excellent agreement of results are achieved using a total of twenty modes in each region where three modes in each transformer section are interacting modes.

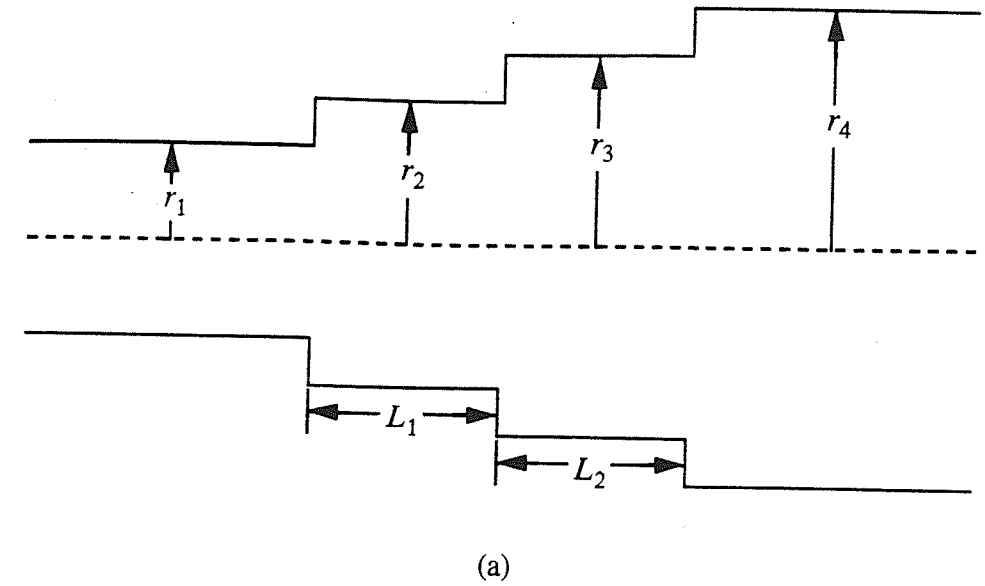

(a)

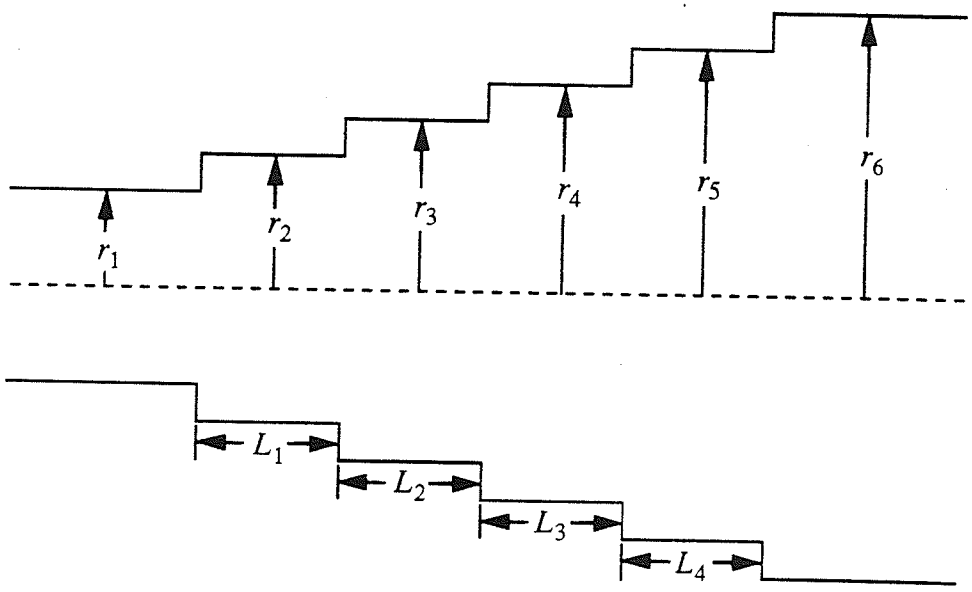

(b)

Fig. 4.3. Geometry of a circular waveguide step transformer.
a) two-section transformer
b) four-section transformer

Table 4.9

Dimensions for step transformer designs.

(in cm)

	Two-section Transformer	Four-section Transformer
r_1	1.1165	1.1165
r_2	1.1360	1.1210
r_3	1.1965	1.1415
r_4	1.3400	1.1685
r_5		1.2090
r_6		1.3400
L_1	1.3610	1.3990
L_2	1.2410	1.3480
L_3		1.2930
L_4		1.2270

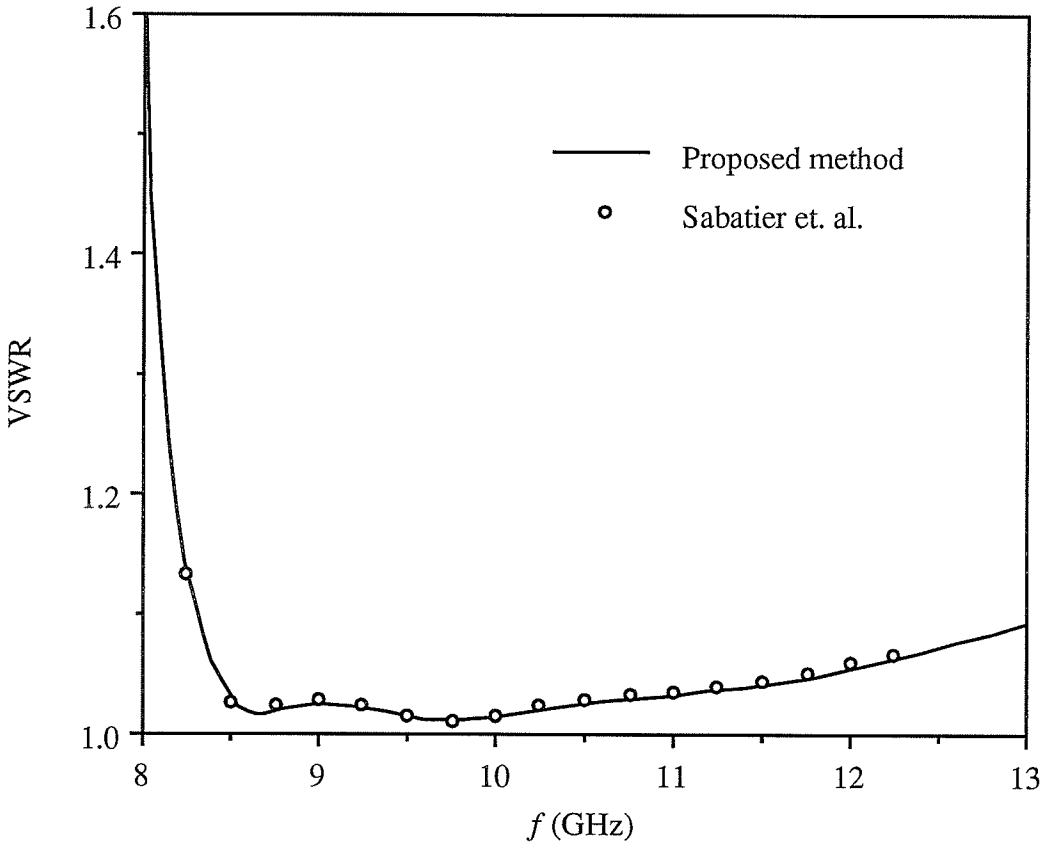

Fig. 4.4. VSWR of a two-section transformer with dimensions as in Table 4.9.

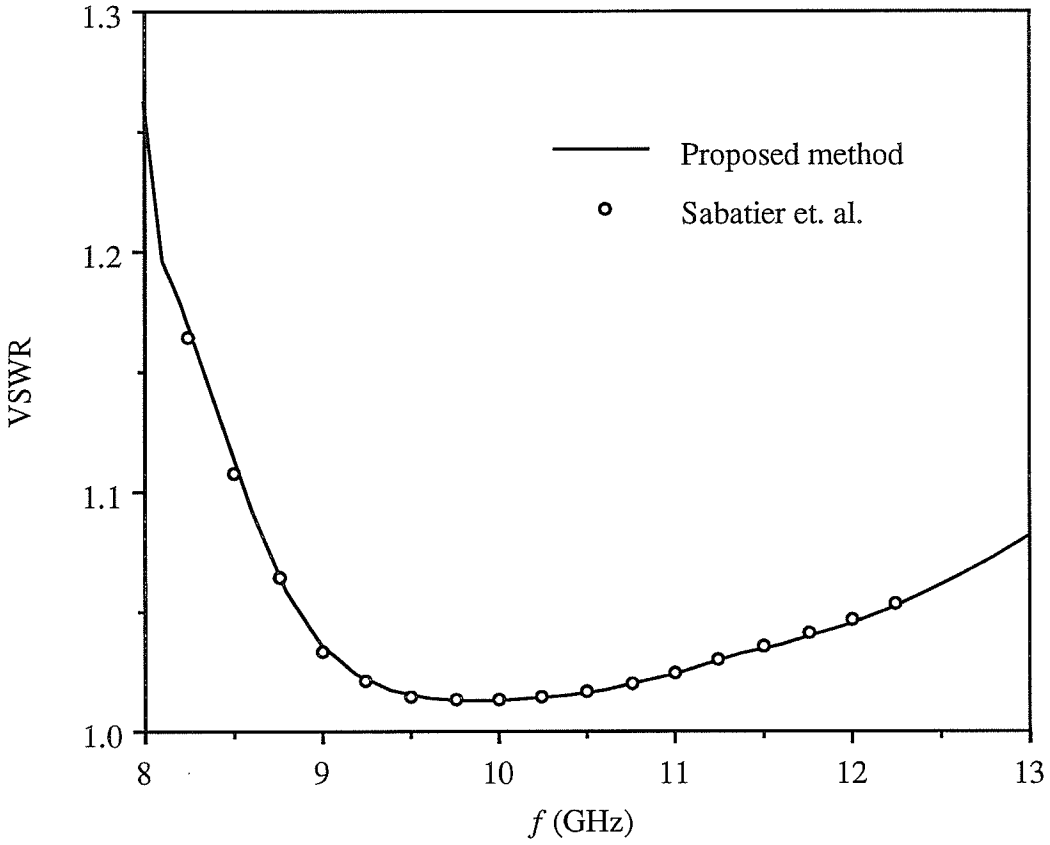

Fig. 4.5. VSWR of a four-section transformer with dimensions as in Table 4.9.

CHAPTER 5

CONCLUSIONS AND RECOMMENDATIONS

In this thesis, a general solution for the scattering from multiple discontinuities in waveguides has been presented. The global scattering matrices are calculated by simultaneously solving for the interaction between the discontinuities using a recurrence procedure rather than by cascading individual discontinuities. Compared with the commonly used cascading techniques, the proposed formulation has a significant computational advantage by requiring fewer matrix multiplications and inversions for the calculation of the scattering matrices.

In Chapter 3, the formulation was applied to step-discontinuities in circular waveguides for quantitative studies. It was found that the ratio of the number of modes in each region should be chosen approximately equal to the ratio of the waveguide cross section dimensions to ensure a very rapid convergence of results. In the case of closely separated discontinuities, this choice for the mode ratio is critical for achieving accurate results. The accuracy of the proposed formulation has been confirmed by comparing numerical results for a thick iris in a circular waveguide with data available in the literature. The computation for the thick iris required only one relatively small matrix inversion while two 40 x 40 matrix inversions were required for the moment method solution [14].

Previously published designs for iris matched dielectric windows [18] were calculated using a relatively small modes that was insufficient to account for the higher order mode interaction of closely spaced discontinuities. By using a larger number of modes in the ratio of the dimensions, designs have been improved by as much as 4.2 percent. The frequency response for the improved designs have also been calculated and presented.

The analysis in Chapter 2 takes into account the near field coupling and higher order mode interaction between discontinuities. However, the formulation has been modified in Chapter 4 to eliminate the coupling of the higher order modes that do not effectively interact with the adjacent discontinuities. This extends the applicability of the formulation to cases with large separation distances between discontinuities. For the linear dimensions considered, the evanescent modes with $\gamma L < 4$ were found to be effectively interacting between the discontinuities and should be included in the truncations. Numerical results for a thick iris in a circular waveguide and for multiple-step transformers in circular waveguides have been compared with data available in the literature to confirm the accuracy of the modified formulation.

Although only step-discontinuities in circular waveguides have been discussed in this thesis, the formulation can be applied to general transverse discontinuities in waveguides of any cross section. The conditions for good convergence for waveguides of other cross section would be expected to be similar to the criterion described here, but this needs to be verified.

APPENDIX

IDENTITIES FOR COUPLING MATRICES

Consider the matrix equations for a single boundary reduction discontinuity

$$\underline{A}_1 + \underline{B}_1 = \underline{\underline{Z}}^T \underline{B}_2$$

$$\underline{\underline{Z}} (\underline{A}_1 - \underline{B}_1) = \underline{B}_2 \tag{1}$$

where $\underline{A}_1$ is the incident excitation, and $\underline{B}_1$ and $\underline{B}_2$ are the unknown reflected and transmitted coefficients, respectively. Solving for $\underline{B}_1$ and $\underline{B}_2$ it can be shown that

$$\underline{B}_1 = -\left(\underline{\underline{I}} + \underline{\underline{Z}}^T \underline{\underline{Z}} \right)^{-1} \left(\underline{\underline{I}} - \underline{\underline{Z}}^T \underline{\underline{Z}} \right) \underline{A}_1$$

$$\underline{B}_2 = 2 \left(\underline{\underline{I}} + \underline{\underline{Z}}^T \underline{\underline{Z}} \right)^{-1} \underline{\underline{Z}} \, \underline{A}_1 \tag{2}$$

Substituting $\underline{B}_1$ and $\underline{B}_2$ into the first equation of (1) and simplifying gives

$$\underline{\underline{I}} - \left(\underline{\underline{I}} + \underline{\underline{Z}}^T \underline{\underline{Z}} \right)^{-1} \left(\underline{\underline{I}} - \underline{\underline{Z}}^T \underline{\underline{Z}} \right) \equiv 2 \left(\underline{\underline{I}} + \underline{\underline{Z}}^T \underline{\underline{Z}} \right)^{-1} \tag{3}$$

or

$$\underline{\underline{I}} + \left(\underline{\underline{I}} + \underline{\underline{Z}}^T \underline{\underline{Z}} \right)^{-1} \left(\underline{\underline{I}} - \underline{\underline{Z}}^T \underline{\underline{Z}} \right) \equiv 2\underline{\underline{I}} - 2\underline{\underline{Z}}^T \left(\underline{\underline{I}} + \underline{\underline{Z}}^T \underline{\underline{Z}} \right)^{-1} \underline{\underline{Z}} \tag{4}$$

From the left hand side of (4), it can be shown that

$$\underline{\underline{I}} + \left(\underline{\underline{I}} + \underline{\underline{Z}}^T \underline{\underline{Z}} \right)^{-1} \left(\underline{\underline{I}} - \underline{\underline{Z}}^T \underline{\underline{Z}} \right) \equiv 2 \left(\underline{\underline{I}} + \underline{\underline{Z}}^T \underline{\underline{Z}} \right)^{-1} \tag{5}$$

Comparing (4) and (5), it is apparent that

$$\left(\underline{\underline{I}} + \underline{\underline{Z}}^T \underline{\underline{Z}} \right)^{-1} \equiv \underline{\underline{I}} - \underline{\underline{Z}}^T \left(\underline{\underline{I}} + \underline{\underline{Z}}^T \underline{\underline{Z}} \right)^{-1} \underline{\underline{Z}} \tag{6}$$

From the matrix equations for a single boundary enlargement, it can be shown that (5) and (6) are valid for $\underline{\underline{Z}}$ replaced by $\underline{\underline{Z}}^T$, where $\underline{\underline{Z}} \equiv \underline{\underline{G}}, \underline{\underline{P}}, \underline{\underline{H}}, \underline{\underline{K}}$.

REFERENCES

1. G. Matthaei, L. Young, and E. M. T. Jones, *Microwave Filters, Impedance-Matching Networks, and Coupling Structures.* New York: McGraw-Hill, 1964.

2. G. L. James, "Analysis and design of TE_{11}-to-HE_{11} corrugated cylindrical waveguide mode converters," *IEEE Trans. Microwave Theory Tech.*, vol. MTT-29, no. 10, pp. 1059-1066, Oct. 1981.

3. K. Raghavan, A. D. Olver, and P. J. B. Clarricoats, "Compact dual-mode dielectric loaded horn," *Electronics Letters*, vol. 22, no. 21, pp. 1131-1132, Oct. 9, 1986.

4. T. S. Chu and T. Itoh, "Generalized scattering matrix method for analysis of cascaded and offset microstrip step discontinuities," *IEEE Trans. Microwave Theory Tech.*, vol. MTT-34, no. 2, pp. 280-284, Feb. 1986.

5. A. S. Omar and K. Schünemann, "Transmission matrix representation of finline discontinuities," *IEEE Trans. Microwave Theory Tech.*, vol. MTT-33, no. 9, pp. 765-770, Sept. 1985.

6. R. Mittra and S. W. Lee, *Analytical Techniques in the Theory of Guided Waves.* New York: Macmillan, 1971.

7. M. Leroy, "On the convergence of numerical results in modal analysis," *IEEE Trans. Antennas Propagat.*, vol. AP-31, no. 4, pp. 655-659, July 1983.

8. R. R. Mansour and R. H. MacPhie, "An improved transmission matrix formulation of cascaded discontinuities and its application to *E*-plane circuits," *IEEE Trans. Microwave Theory Tech.*, vol. MTT-34, no. 12, pp. 1490-1498, Dec. 1986.

9. F. Alessandri, G. Bartolucci, and R. Sorrentino, "Admittance matrix formulation of waveguide discontinuity problems: computer-aided design of branch guide directional couplers," *IEEE Trans. Microwave Theory Tech.*, vol. MTT-36, no. 2, pp. 394-403, Feb. 1988.

10. T. E. Rozzi and W. F. G. Mecklenbräuker, "Wide-band network modeling of interacting inductive irises and steps," *IEEE Trans. Microwave Theory Tech.*, vol. MTT-23, no. 2, pp. 235-245, Feb. 1975.

11. R. De Smedt and B. Denturck, "Scattering matrices of junctions between rectangular waveguides," *IEE Proc.*, vol. 130 Pt. H, no. 2, Mar. 1983.

12. A. K. Hamid, I. R. Ciric, and M. Hamid, "Moment method solution of double step discontinuities in waveguides," *Int. J. Electronics*, vol. 65, no. 6, pp. 1159-1169, 1988.

13. A. Datta, B. N. Das, and A. Chakraborty, "Moment method formulation of thick diaphrams in a rectangular waveguide," *IEEE Trans. Microwave Theory Tech.*, vol. MTT-40, no. 3, pp. 592-595, Mar. 1992.

14. R. W. Scharstein and A. T. Adams, "Galerkin solution for the thin circular iris in a TE_{11}-mode circular waveguide," *IEEE Trans. Microwave Theory Tech.*, vol. MTT-36, no. 1, pp. 106-113, Jan. 1988.

15. P. J. B. Clarricoats and K. R. Slinn, "Numerical solution of waveguide-discontinuity problems," *Proc. IEE*, vol. 114, no. 7, pp. 878-886, July 1967.

16. P. R. Huckle and P. H. Masterman, "Analysis of a rectangular waveguide junction incorporating a row of rectangular posts," *Electronics Letters*, vol. 5, no. 22, Oct. 30, 1969.

17. A. Wexler, "Solution of waveguide discontinuities by modal analysis," *IEEE Trans. Microwave Theory Tech.*, vol. MTT-15, no. 9, pp. 508-517, Sept. 1967.

18. L. Carin, K. J. Webb, and S. Weinreb, "Matched windows in circular waveguide," *IEEE Trans. Microwave Theory Tech.*, vol. MTT-36, no. 9, pp. 1359-1362, Sept. 1981.

19. G. Gesell and I. R. Ciric, "Scattering from double discontinuities in circular waveguides," *IEEE Antennas Propagat. Soc. Int. Symp.*, Chicago, July 1992.

20. G. Gesell and I. R. Ciric, "A novel recurrence modal analysis formulation for multiple waveguide discontinuities," *Proc. Antennas and Applied Electromagnetics Symp.*, University of Manitoba, Winnipeg, Canada, Aug. 1992.

21. G. Gesell and I. R. Ciric, "Recurrence modal analysis for multiple waveguide discontinuities and its application to circular structures," *IEEE Trans. Microwave Theory Tech.* (submitted).

22. R. E. Collin, *Field Theory of Guided Waves*. New York: McGraw-Hill, 1960.

23. A. Z. Elsherbeni, J. Stanier, and M. Hamid, "Eigenvalues of propagating waves in a circular waveguide with an impedance wall," *IEE Proc.*, vol. 135, Pt. H, no.1, Feb. 1988.

24. P. H. Masterman and P. J. B. Clarricoats, "Computer field-matching solution of waveguide transverse discontinuities," *Proc. IEE*, vol. 118, no. 1, pp. 51-63, Jan. 1971.

25. International Mathematical and Statistical Library, Problem Solving Software System for Mathematical and Statistical Fortran programming, 1985.

26. C. Sabatier, R. Behe, and P. Brachat, "Approximate formulas for step-discontinuities in circular waveguides," *Electronics Letters*, vol. 5, no. 3, Feb. 1, 1990.